Engineering of Flavin-Binding Proteins for Superresolution and Bioluminescence Microscopy

Von der Naturwissenschaftlichen Fakultät der
Gottfried Wilhelm Leibniz Universität Hannover

zur Erlangung des Grades
Doktorin der Naturwissenschaften (Dr. rer. nat.)

genehmigte Dissertation
von
M.Sc. Anne Carola Gregor

geboren am 18.12.1986 in Hannover

2018

Referent: Prof. Dr. Anaclet Ngezahayo

Korreferent: Prof. Dr. Stefan Hell

Tag der Promotion: 26.09.2016

Abstract

Live cell imaging is an important tool for the investigation of cellular processes. It has become possible with the discovery and improvement of fluorescent proteins that can be genetically fused to a protein of interest, thereby allowing its direct observation by fluorescence microscopy. The resolution of conventional fluorescence microscopy is limited by diffraction to ~200 nm which is not sufficient for the detailed analysis of cellular organelles. Several methods that bypass the diffraction limit have been developed, including STED (stimulated emission depletion) and RESOLFT (reversible saturable optical linear fluorescence transition) microscopy which allow imaging of living cells far beyond the diffraction limit. RESOLFT microscopy uses reversibly switchable fluorescent proteins (RSFPs) to obtain increased resolution. All commonly used RSFPs have been developed from fluorescent proteins of the GFP (green fluorescent protein) family. These proteins exhibit high brightness, but are not optimal for all applications due to their relatively large size (27 kDa), dependence on oxygen for chromophore maturation, and fluorescence quenching at low pH. Another class of fluorescent proteins that circumvents all these problems are LOV (light-oxygen-voltage-sensing) domains that contain a flavin chromophore. In the first project of this thesis, two new RSFPs were developed from the LOV domain of the photoreceptor protein YtvA from *Bacillus subtilis* by mutagenesis. The first variant rsLOV1 was successfully used for RESOLFT imaging, whereas the second variant rsLOV2 was used for STED microscopy achieving a resolution of down to 40–50 nm in living cells.

Another type of flavin-binding proteins that can also be used for imaging are bacterial luciferases. These enzymes use FMN (flavin mononucleotide) to convert chemical energy into light in a process called bioluminescence. The emitted light can be used for imaging without an external light source as it is required for the excitation of fluorescence, which can disturb light-sensitive processes and lead to photobleaching. However, the low brightness of bacterial bioluminescence has so far limited its use for single-cell imaging. In the second part of this thesis, it was shown that bioluminescence from the *luxCDABE* operon from *Photorhabdus luminescens* could be improved ~7-fold by expression of an additional FMN reductase and subsequent mutagenesis of several proteins of the *lux* operon. The resulting *ilux* operon could be used to image single *E. coli* cells for extended time periods at enhanced spatiotemporal resolution and to investigate the effect of different antibiotics on cell viability.

Zusammenfassung

Die Beobachtung lebender Zellen ist eine wichtige Methode zur Erforschung zellulärer Prozesse. Sie wurde möglich durch die Entdeckung und Verbesserung fluoreszierender Proteine, welche genetisch an zelluläre Proteine fusioniert werden können und so deren direkte Beobachtung durch Fluoreszenzmikroskopie ermöglichen. Die Auflösung herkömmlicher Fluoreszenzmikroskope ist durch Beugung auf etwa 200 nm begrenzt. Dies ist für die detaillierte Beobachtung von Zellorganellen nicht ausreichend. Es wurden jedoch mehrere Methoden entwickelt, die das Beugungslimit umgehen. Zu diesen gehören die STED (*stimulated emission depletion*)- und RESOLFT (*reversible saturable optical linear fluorescence transition*)-Mikroskopie, welche die Beobachtung lebender Zellen mit einer Auflösung deutlich unterhalb der Beugungsgrenze ermöglichen. Die RESOLFT-Mikroskopie verwendet reversibel schaltbare fluoreszierende Proteine (RSFPs) zur Verbesserung der Auflösung. Alle bisher gebräuchlichen RSFPs wurden aus Proteinen der GFP (grün fluoreszierendes Protein)-Familie entwickelt. Diese Proteine besitzen eine hohe Helligkeit, sind jedoch aufgrund ihrer relativ hohen Größe (27 kDa), Sauerstoff-Abhängigkeit und Empfindlichkeit ihrer Fluoreszenz gegenüber niedrigen pH-Werten nicht für alle Anwendungen geeignet. Eine andere Klasse fluoreszierender Proteine, die alle diese Probleme umgeht, sind LOV (*light-oxygen-voltage-sensing*)-Domänen, welche einen Flavin-Chromophor enthalten. Im ersten Projekt dieser Arbeit wurden zwei neue RSFPs durch Mutagenese ausgehend von der LOV-Domäne des Photorezeptor-Proteins YtvA aus *Bacillus subtilis* entwickelt. Die erste Variante rsLOV1 wurde für RESOLFT-Mikroskopie verwendet, während mit der zweiten Variante rsLOV2 durch STED-Mikroskopie eine Auflösung von 40–50 nm in lebenden Zellen erreicht werden konnte.

Ein weiterer Typ Flavin-bindender Proteine, die ebenfalls zur Abbildung lebender Zellen verwendet werden können, sind bakterielle Luciferasen. Diese Enzyme verwenden FMN (Flavinmononukleotid), um chemische Energie in einem als Biolumineszenz bezeichneten Prozess in Licht umzuwandeln. Anders als Fluoreszenz kann die Emission von Biolumineszenz ohne zusätzliches Licht von außerhalb aufgenommen werden, welches lichtempfindliche Prozesse stören und zu Bleichen führen kann. Die Verwendbarkeit bakterieller Biolumineszenz zur Abbildung einzelner Zellen wurde jedoch bisher durch ihre geringe Helligkeit eingeschränkt. Im zweiten Teil dieser Arbeit wurde gezeigt, dass die Biolumineszenz vom *luxCDABE*-Operon aus *Photorhabdus luminescens* etwa 7-fach erhöht werden konnte. Dies wurde durch die zusätzliche Expression einer FMN-Reduktase und

anschließende Mutagenese mehrerer Proteine des *lux*-Operons erreicht. Das verbesserte *ilux*-Operon konnte zur Beobachtung einzelner *E. coli*-Zellen mit erhöhter räumlich-zeitlicher Auflösung über lange Zeiträume verwendet werden und ermöglichte darüber hinaus die Erforschung der Wirkung verschiedener Antibiotika auf die Zellviabilität.

Disclaimer

Parts of the here presented work are already published in peer-reviewed articles. These are modified versions of chapters I and II as follows:

Gregor C, Sidenstein SC, Andresen M, Sahl SJ, Danzl JG, Hell SW
Novel reversibly switchable fluorescent proteins for RESOLFT and STED nanoscopy engineered from the bacterial photoreceptor YtvA
Scientific Reports **8**(1), 2724 (2018)

Gregor C, Gwosch KC, Sahl SJ, Hell SW
Strongly enhanced bacterial bioluminescence with the *ilux* operon for single-cell imaging
PNAS, **115**(5), 962-967 (2018)

Table of Contents

Abbreviations

aa	amino acid
ATP	adenosine-5'-triphosphate
BLUF domain	sensors of blue light using FAD
B. subtilis	*Bacillus subtilis*
CCD	charge-coupled device
DNA	deoxyribonucleic acid
E. coli	*Escherichia coli*
e.g.	for example
EMCCD	electron-multiplying charge-coupled device
FAD, FADH$_2$	flavin adenine dinucleotide
FbFP	FMN-binding fluorescent protein
FMN, FMNH$_2$	flavin mononucleotide
FRET	Förster resonance energy transfer
FWHM	full width at half maximum
GFP	green fluorescent protein
GTP	guanosine-5'-triphosphate
ICCD	intensified charge-coupled device
IPTG	isopropyl β-D-1-thiogalactopyranoside
LB	lysogeny broth
LOV domain	light-oxygen-voltage-sensing domain
NAD$^+$, NADH	nicotinamide adenine dinucleotide
NADP$^+$, NADPH	nicotinamide adenine dinucleotide phosphate
OD$_{600}$	optical density at 600 nm
PALM	photoactivated localization microscopy
PCR	polymerase chain reaction
PDB	protein data bank
PI	propidium iodide
P$_i$	inorganic phosphate
P. luminescens	*Photorhabdus luminescens*
PP$_i$	pyrophosphate
RESOLFT	reversible saturable optical linear fluorescence transition
RF	riboflavin

Abbreviations

|	
SNR	signal-to-noise ratio
RSFP	reversibly switchable fluorescent protein
STED	stimulated emission depletion
VBNC	viable but non-culturable
V. campbellii	*Vibrio campbellii*
V. harveyi	*Vibrio harveyi*
YFP	yellow fluorescent protein

Introduction

Light microscopy has become an indispensable tool for cell biology. With the discovery and development of new fluorescent proteins during the last decades, it became possible to specifically label proteins in living cells and to image them in their native environment. The resolution of light microscopy, however, is typically limited to ~200 nm due to diffraction. Various cellular organelles such as endosomes are considerably smaller than 200 nm, making it impossible to resolve their structure with conventional light microscopes. Higher resolution in the sub-nanometer range can be achieved with electron microscopy. Unfortunately, this technique requires previous fixation and staining of the sample and is therefore not compatible with live cell imaging. In addition, the fixation procedure can lead to the creation of artifacts. During the last decades, several methods based on fluorescence microscopy have been developed that allow imaging of living cells far beyond the diffraction limit, including STED (stimulated emission depletion) and RESOLFT (reversible saturable optical linear fluorescence transition) microscopy. These methods require suitable fluorophores. Fluorescent proteins for live cell imaging with STED and RESOLFT microscopy have so far been mainly developed from GFP (green fluorescent protein) and related proteins. Yet, other proteins with entirely different properties exist that contain a fluorescent cofactor and can therefore also be used for fluorescence microscopy. One of these proteins are flavin-binding LOV (light-oxygen-voltage-sensing) domains that are superior to GFP-based proteins for certain applications due to their smaller size, oxygen-independence, and stability of their fluorescence at low pH [1]. Chapter I of this thesis deals with the development of LOV-based proteins for RESOLFT and STED microscopy.

Flavin-binding proteins can also be used for another type of imaging. Several bacteria use FMN (flavin mononucleotide) to convert chemical energy into light in a process called bioluminescence. Hence, detection of the emitted light allows imaging without an external light source. This is particularly useful for long-term measurements of living cells where phototoxicity and bleaching of fluorescent proteins can be a problem. However, due to its low light intensity, imaging of bacterial bioluminescence suffers from poor spatiotemporal resolution. Chapter II of this work therefore focuses on the improvement of bioluminescence emission for long-term studies on the single cell level.

The following paragraphs provide the theoretical background for chapter I and II.

Flavins

Flavins are a group of cellular redox cofactors that contain an isoalloxazine ring system. They include riboflavin (RF), also known as vitamin B_2, and its biologically active derivatives flavin mononucleotide (FMN) and flavin adenine dinucleotide (FAD) (Figure 1). Whereas plants and most bacteria are able to synthesize riboflavin from GTP (guanosine-5'-triphosphate) and ribulose 5-phosphate [2] (p. 15), animals must take up riboflavin contained in their diet or produced by intestinal bacteria. Riboflavin is absorbed by carrier proteins [3] and phosphorylated by riboflavin kinase to FMN which can be further converted into FAD by FAD synthetase.

(a)

isoalloxazine

(b)

RF   FMN   FAD
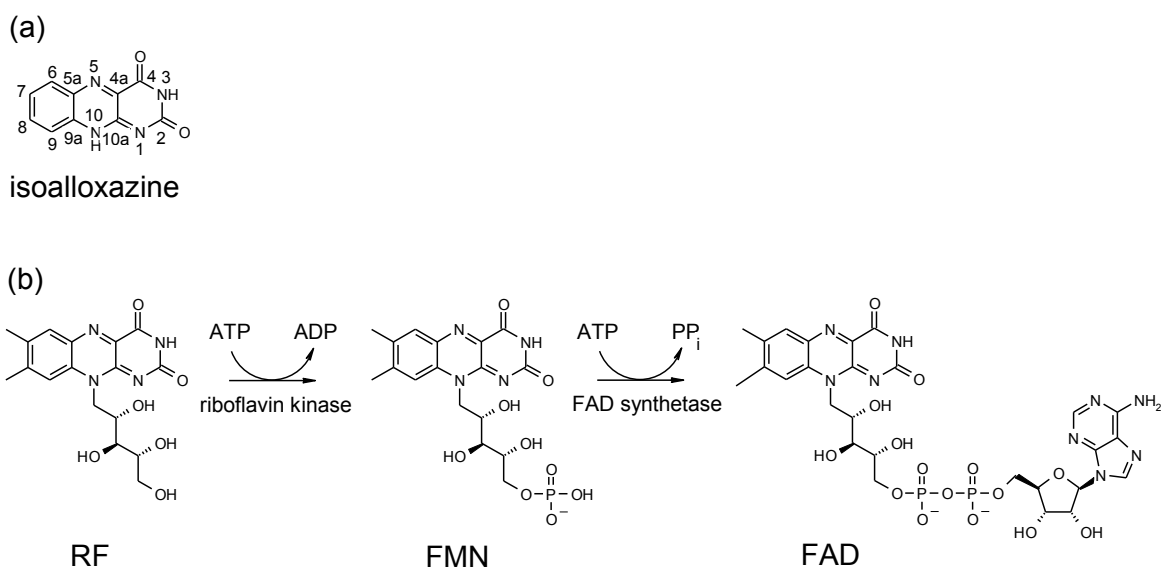
**Figure 1: Structures of different flavins**

(a) Structure of isoalloxazine

(b) Structures and interconversion of RF, FMN, and FAD

FMN and FAD are found in a large number of flavoproteins to which they are usually non-covalently bound. Due to their unique ability to mediate both one- and two-electron redox reactions, they are important for many cellular oxidation/reduction reactions. For instance, FMN and FAD are required for several one- and two-electron transfer processes in the citric acid cycle and respiratory chain [4] (pp. 786-788 and 808 f) and photosynthesis [4] (p. 893). In addition, flavins are involved in fatty acid oxidation [4] (pp. 916 f), halogenation reactions [5], and photorepair of DNA damage [6, 7]. Flavins also serve as the blue light-sensing component in different photoreceptors such as LOV and BLUF (sensors of blue light using

FAD) domains (see chapter I). Furthermore, FMN is required for generation of bacterial bioluminescence (see chapter II).

The three different redox states of flavins (oxidized, one-electron reduced (semiquinone), and fully reduced (hydroquinone)) exist as a mixture of different protonation states in solution (Figure 2). At pH 7, the redox potential for the two-electron reduction of free flavins is about E_m = -200 mV [2] (p. 6). However, the redox potential of protein-bound flavins can be substantially different, ranging from about -500 mV to +80 mV [2] (p. 230), [8], demonstrating the important role of the flavin environment. The redox potential is expected to decrease in a hydrophobic environment or with negative charges nearby, whereas positive charges are believed to increase it [2] (p. 6), [9]. In the excited state, the redox potential strongly increases to 1.9 V [10], favoring electron transfer reactions (see below).
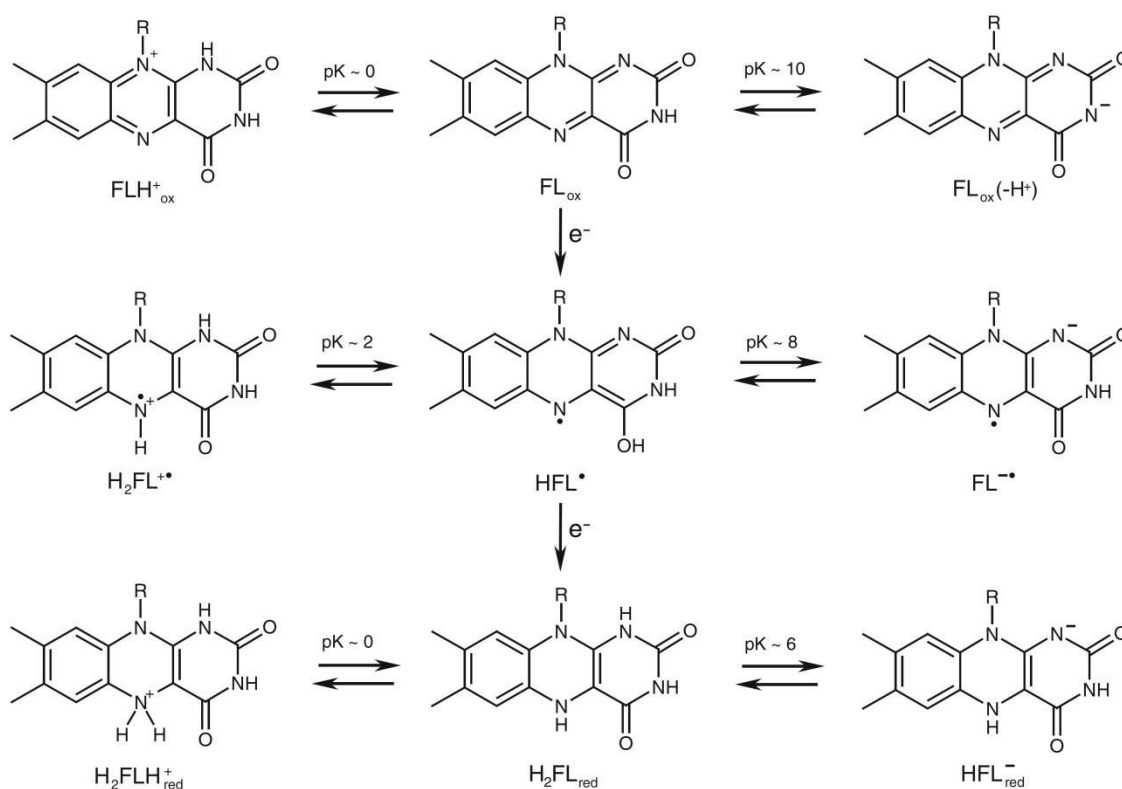
Figure 2: Redox and acid-base equilibria of flavins (FL) [2] (p. 6)

The oxidized form of flavins strongly absorbs in the UV and blue region with absorption peaks at 445, 375, 265, and 220 nm [2] (p. 8) (Figure 3a). The extinction coefficient of riboflavin at 445 nm in water is 12,500 $M^{-1} \cdot cm^{-1}$ [11]. Neutral, oxidized flavins in aqueous solution exhibit strong fluorescence with a maximum at ~520 nm (Figure 3b) whereas the protonated and

deprotonated forms are non-fluorescent [2] (p. 9). The fluorescence quantum yields are 0.27 for riboflavin and FMN and 0.04 for FAD due to quenching by its adenosyl moiety [12]. Despite the strong fluorescence of flavins in solution, many flavin-binding proteins are only very weakly fluorescent or non-fluorescent. The reason for this are electron transfer and electron transfer followed by proton transfer reactions from nearby tryptophan and tyrosine residues to the excited flavin chromophore [13, 14], [15] (pp. 315 f). Nevertheless, some flavoproteins exhibit relatively bright fluorescence, including the LOV domains described in the following section.

(a)　　　　　　　　　　　　　　　　　　(b)
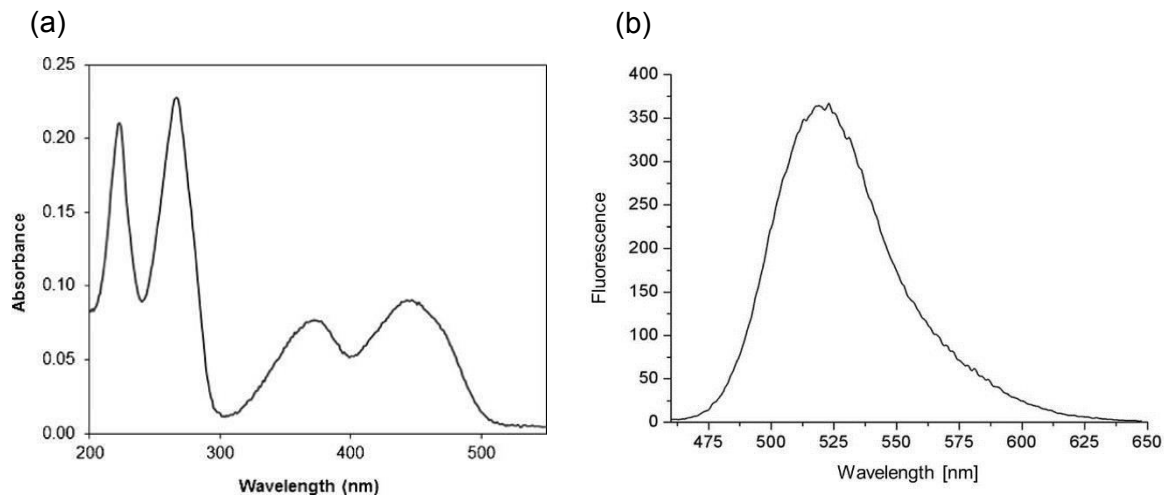
Figure 3: Absorption and fluorescence emission spectra of riboflavin

(a) Absorption spectrum of riboflavin [16]

(b) Fluorescence spectrum of riboflavin excited at 450 nm (adapted from [17])

Photoreceptor Proteins and LOV Domains

To be able to sense and respond to light, living organisms possess several types of photoreceptor proteins. These proteins usually contain a chromophore that absorbs light in a certain spectral range, thereby triggering a conformational change in the protein which leads to a cellular response. Some examples for photoreceptors are rhodopsins in the vertebrate retina for visual perception and cryptochromes, phototropins, and phytochromes in plants that control for instance time of flowering, phototropism, and photomorphogenesis [18, 19]. Whereas phytochromes contain a bilin chromophore for the reception of red light, cryptochromes and phototropins both bind flavin chromophores and absorb light in the blue region. Phototropins contain LOV domains as their flavin-binding moiety which non-covalently bind oxidized FMN (in some cases FAD) [20]. LOV domains are not only found in plants, but also in fungi and bacteria, where they are coupled to different effector domains that mediate

6

the cellular response, such as histidin kinases and serine/threonine kinases. The LOV domain of the bacterial photoreceptor protein YtvA from *Bacillus subtilis* that is used in chapter I of this work contains a STAS (sulphate transporter anti-σ antagonist) effector domain that is involved in general stress response [20, 21].

The light-dependent signaling from the LOV domain to the effector domain functions in different ways. In YtvA, signal transmission is achieved by rotation of its two LOV domains relative to each other by 5° [22]. Signaling in the AsLOV2 domain of *Avena sativa* phototropin involves partial unfolding of an α-helix, whereas the LOV protein Vivid forms homodimers upon illumination [20, 23, 24]. Despite these entirely different effects, all LOV domains share the underlying mechanism of light sensing and undergo a photocycle that is shown in a simplified version in Figure 4a (see [25] for a more detailed description of the photocycle of YtvA-LOV). Upon absorption of blue light, the FMN that is first non-covalently bound to the LOV domain is excited into a triplet state. Subsequently, a covalent bond between the FMN and a cysteine residue of the protein is formed, possibly via a semiquinone form of the FMN. Upon bond formation, the plane of the FMN ring system is tilted by ~6° towards the cysteine residue [22], leading to the rearrangement of the surrounding residues of the binding pocket (Figure 4b). This triggers a small conformational change in the whole protein that mediates the downstream signaling. After several seconds to hours ($\tau = 43\ min$ at room temperature for YtvA-LOV [25]), the photoadduct decays back to the non-covalently bound state.
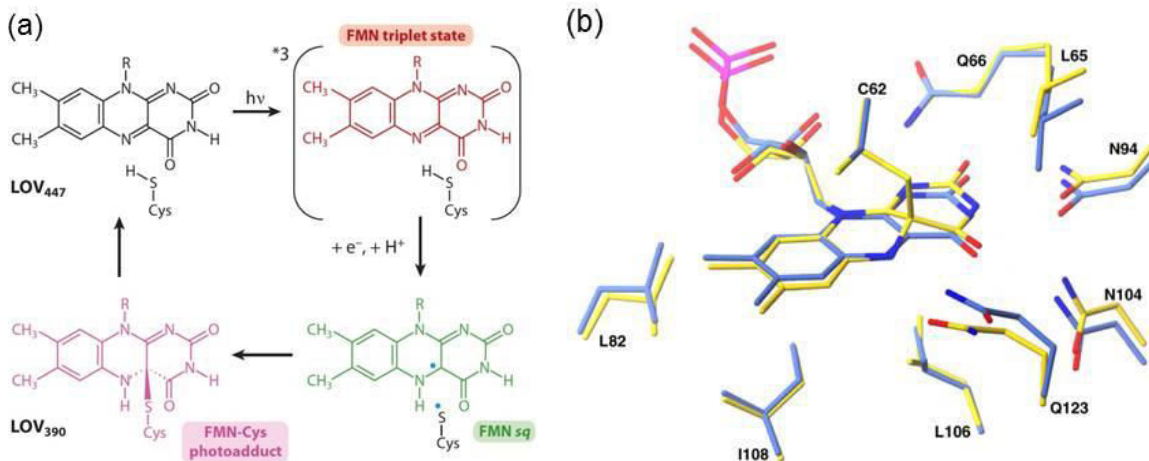
Figure 4: Photocycle of LOV domains

(a) (from [10]) Absorption of blue light by FMN triggers the formation of a covalent bond to a cysteine residue of the protein. The photoadduct decays spontaneously into the non-covalently bound state.

(b) Comparison of the FMN binding pocket of YtvA-LOV in the dark- (blue) and light-adapted state (yellow) (adapted from [22])

YtvA consists of an N-terminal segment (amino acids (aa) 1–24), a LOV domain (aa 25–126), a linker region (aa 127–147), and a C-terminal STAS domain (aa 148–258) [22]. The structures of YtvA-LOV (aa 20–147) in the dark- and light-adapted state and the recently solved structure of the full-length YtvA protein are shown in Figure 5. The isolated LOV domain with and without the N-terminal extension (aa 1–126 and aa 25–126) has a strong tendency to dimerize via a hydrophobic β-sheet [26]. However, dimerization of full-length YtvA in solution is prevented by its C-terminal domain [26]. The FMN is bound to the LOV domain by hydrogen bonds and hydrophobic interactions with multiple residues of the binding pocket. The affinity of YtvA-LOV for FMN is ~715 nM [27].
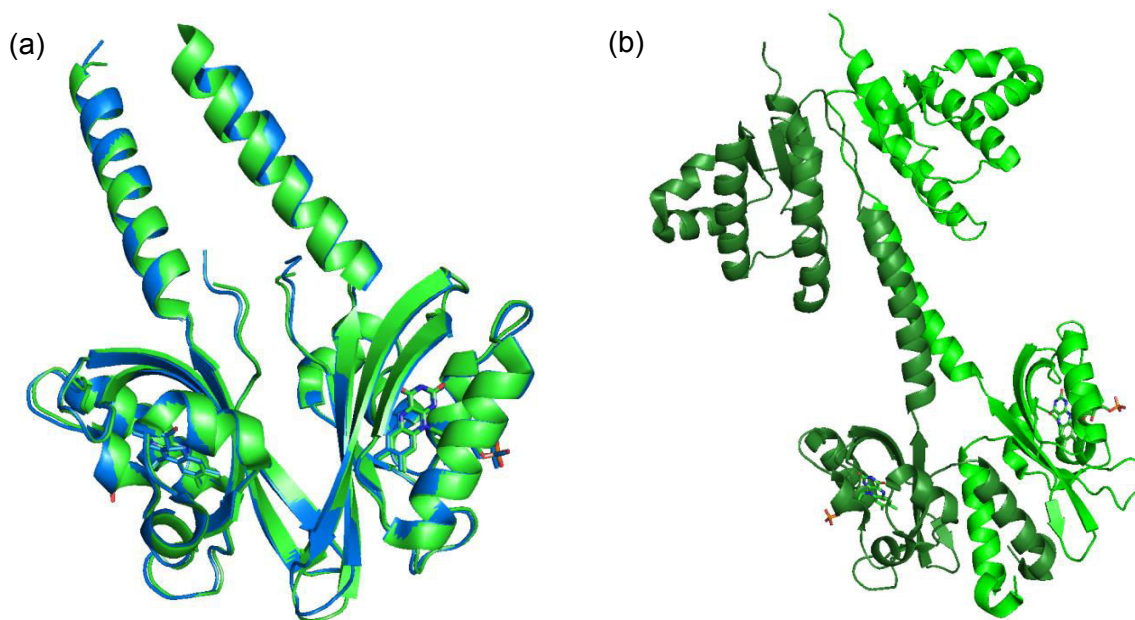
Figure 5: Structure of the photoreceptor YtvA
(a) Structures of the dark- (green) and light-adapted form (blue) of YtvA-LOV (PDB (Protein Data Bank) entry 2PR5 and 2PR6 [28])
(b) Structure of full-length YtvA (PDB entry 2MWG [28])

The light-dependent properties of LOV domains make them interesting for two different types of applications. On the one hand, the light-dependent activation of an effector domain can be used for optogenetics. For example, fusion of a LOV domain with the tryptophan repressor protein TrpR from *E. coli* has been demonstrated to enable control of its DNA binding activity by light [29]. On the other hand, LOV domains can be used as fluorescent proteins. Since the FMN is only fluorescent in its oxidized, non-covalently bound form, the photocycle of different LOV domains has been abolished to make these proteins constitutively fluorescent. This was achieved by mutation of the photoactive cysteine residue into an alanine [30-33]. In addition, brighter variants have been generated by DNA shuffling, site-directed and random mutagenesis [31-33]. The resulting FMN-binding fluorescent proteins (FbFPs) include the YtvA-derived protein EcFbFP [30], iLOV and its more photostable variant phiLOV2.1 [31, 32] that were created from *Arabidopsis* phototropin, as well as CreiLOV from *Chlamydomonas reinhardtii* [33]. However, the brightness of FbFPs is still moderate, with extinction coefficients of ~14,000 $M^{-1} \cdot cm^{-1}$ and fluorescence quantum yields in the range of 0.20 to 0.51 [33, 34]. Nevertheless, FbFPs possess several advantages compared to GFP-related proteins. First, their small size (10–19 kDa [31, 35] compared to 27 kDa for EGFP) makes them less likely to influence the function of fusion proteins. In addition, FbFPs are superior for applications where

9

size is limiting, e.g. for packaging into viruses [31]. Second, FbFP fluorescence is oxygen-independent, allowing imaging of anaerobic organisms [30]. Third, fluorescence of FbFPs is preserved at low pH down to pH ~4 [1] where GFP fluorescence is strongly quenched, making them suitable for studying acidic organelles such as lysosomes.

The fluorescence of LOV domains can be excited and switched off by blue light. UV light has been reported to promote cleavage of the photoadduct, converting ~10 % of the proteins back into the fluorescent state [36]. Therefore, LOV domains are promising for the development of new reversibly switchable fluorescent proteins (RSFPs) for superresolution microscopy (see chapter I). First superresolution imaging with a LOV domain has been demonstrated with wild-type YtvA expressed in *E. coli* using photoactivated localization microscopy (PALM) [36].

Bioluminescence

Bioluminescence is a process in living cells that converts chemical energy into light. It is found in certain bacteria, fungi, and animals such as glowworms and fireflies. The functions of bioluminescence include attraction of mates, illumination of prey, camouflage by counterillumination, and defense against predators [37]. There are different ways how bioluminescence light is generated. They all require enzymes referred to as luciferases and their corresponding substrates, luciferins. The luciferase catalyzes the conversion of the luciferin into a product in an electronically excited state that emits a photon upon return to its ground state, thus producing bioluminescence light. Several luciferins are found in nature that are structurally completely distinct, indicating that the phenomenon of bioluminescence has evolved many times independently during evolution. The energy of a photon in the visible range is

$$E = \frac{h \cdot c}{\lambda} \approx \frac{6.6 \cdot 10^{-34} Js \cdot 3.0 \cdot 10^8 ms^{-1}}{500 \; nm} \approx 4 \cdot 10^{-19} J$$

or 240 kJ·mol^{-1}, with h denoting Planck's constant, c the speed of light, and λ the wavelength of the light. This greatly exceeds the free energy of hydrolysis of ATP (adenosine-5'-triphosphate) which is ~50 kJ·mol^{-1} under cellular conditions [4] (p. 567). Since the energy has to be released in a single step, a highly exergonic reaction is required for generation of bioluminescence light. This is achieved by reaction of the luciferin with molecular oxygen for all bioluminescence reactions known so far.

As the excited state of the product of the luciferase reaction is identical to the S_1 state from which fluorescence usually occurs, the bioluminescence emission spectrum is expected to

match the fluorescence spectrum of the product. However, this is rarely the case due to different reasons. First, the spectrum is altered by binding to the luciferase because the energy of the excited state depends on the environment. The second reason is that transfer of the excited state energy to a second molecule can occur. This can either take place by absorption of the bioluminescence light and re-emission of a photon, or in a radiationless process by electron exchange and Förster resonance energy transfer due to dipole-dipole coupling [38]. Several organisms use resonance energy transfer to modulate their bioluminescence emission spectrum. For example, the jellyfish *Aequorea victoria* uses GFP as an acceptor to shift the blue emission from its luciferin coelenterazine to the green. The main function for the energy transfer to an acceptor, however, is assumed to be an increase the overall bioluminescence quantum efficiency since the fluorescence quantum yield of GFP is much higher than for coelenterazine [39].

Most luciferins are only present in organisms expressing the corresponding luciferase. The only exception is the bacterial luciferin $FMNH_2$, the reduced form of FMN that is ubiquitous in all cells. Bacterial bioluminescence is found in several species from the genera *Photobacterium*, *Photorhabdus*, and *Vibrio*. Bioluminescent species of *Photobacterium* and *Vibrio* were isolated from marine habitats whereas the soil bacterium *Photorhabdus* lives symbiotically with entomopathogenic nematodes. All known bacterial luciferases catalyze the same reaction to produce bioluminescence light. In addition to $FMNH_2$, they bind a long chain fatty aldehyde (≥8 carbon atoms) and oxygen. The fatty aldehyde is converted into a fatty acid whereas $FMNH_2$ is oxidized to FMN, thereby emitting blue-green light with λ_{max} ~490 nm (Figure 6). The quantum yield of this reaction is reported to be approximately 10–16 % [40-42].

FMNH$_2$ fatty aldehyde O$_2$ FMN   fatty acid H$_2$O   light
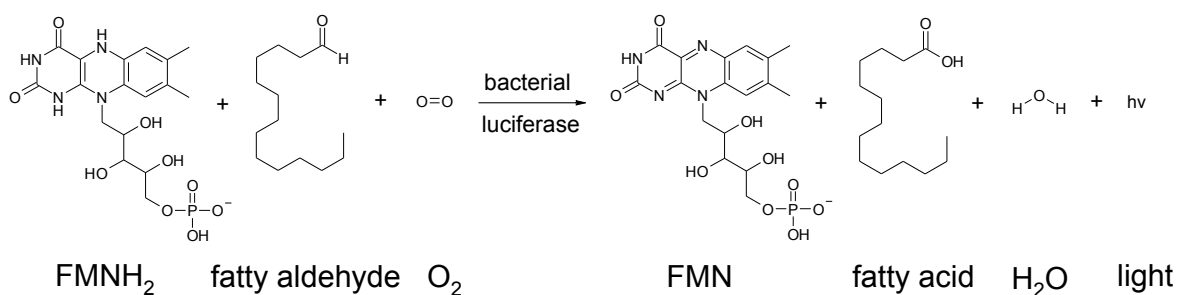
Figure 6: Reaction of bacterial bioluminescence

The mechanism of the bacterial bioluminescence reaction is shown in Figure 7. After binding of FMNH$^-$ to the luciferase, a C4a-peroxyflavin is formed by reaction with oxygen. This

intermediate reacts with the fatty aldehyde to form a flavin-C4a-peroxyhemiacetal. Decay of this adduct results in formation of a carboxylic acid and the luminescence emitter C4a-hydroxyflavin in an excited state. After emission of a photon, the C4a-hydroxyflavin is dehydrated to FMN and both carboxylic acid and FMN are released from the protein [42].
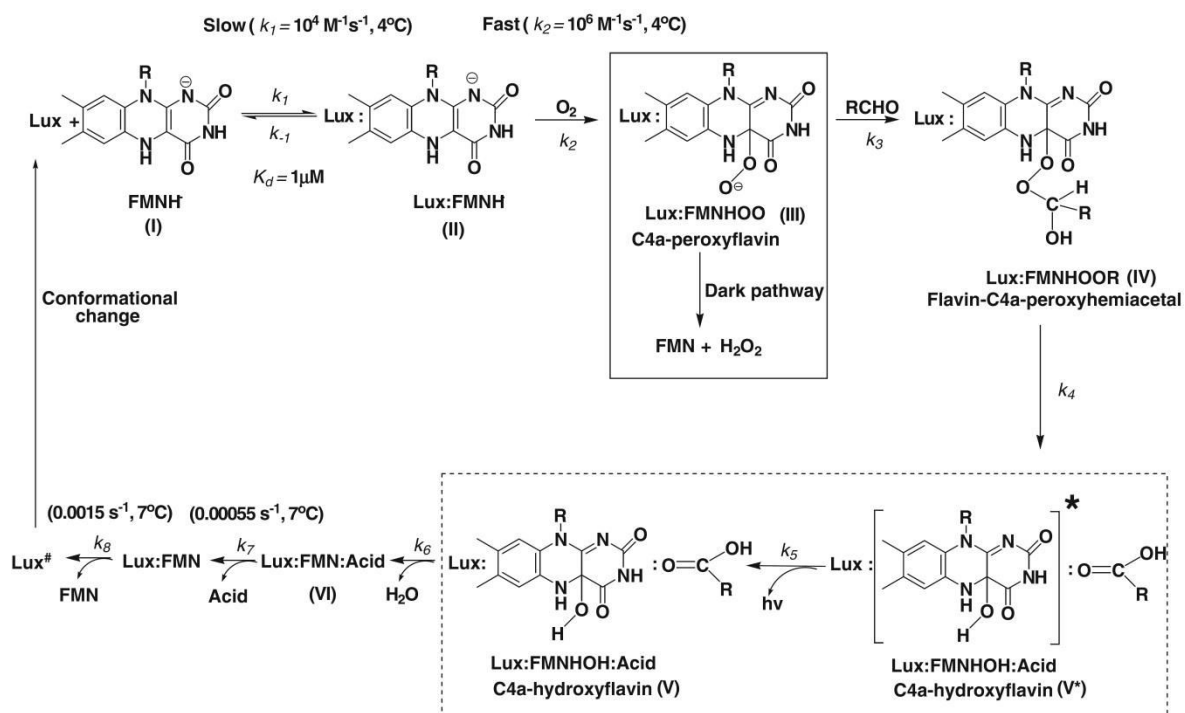

Figure 7: Catalytic mechanism of bacterial luciferase reaction (from [42])

Bacterial luciferase is an αβ heterodimer. The α subunit contains the catalytic center whereas the β subunit serves to stabilize the α subunit, which alone has only very low activity ([43] and references therein). In addition to the luciferase, several other enzymes are required to regenerate the substrates $FMNH_2$ and fatty aldehyde. Reduction of FMN to $FMNH_2$ is catalyzed by an NAD(P)H (nicotinamide adenine dinucleotide (phosphate))-dependent FMN reductase. The fatty aldehyde is regenerated in an ATP- and NADPH-dependent process catalyzed by the fatty acid reductase complex that consists of a fatty acid reductase, a fatty acid transferase, and a fatty acid synthetase. All proteins that are required for generation of bacterial bioluminescence are coded in the *luxCDABE* operon. The *luxA* and *luxB* genes encode the luciferase α and β subunits, whereas *luxC*, *D*, and *E* encode the fatty acid reductase, transferase, and synthetase, respectively. As FMN reductases are also present in non-luminescent bacteria such as *E. coli*, expression of an additional FMN reductase is not necessary for generation of a bioluminescence output. Additional genes in naturally occurring

lux operons serve to regulate bioluminescence. Since generation of bioluminescence light is an energetically demanding process, bacteria only emit bioluminescence light at high cell densities when the resulting signal is high enough to have an impact on their environment. To regulate the emission, bioluminescent bacteria synthesize a cell-permeable autoinducer. At high cell densities, the concentration of the autoinducer increases, leading to enhanced expression of the *luxCDABE* genes and thus to high levels of bioluminescence ([44], [38] and references therein).

Imaging

Superresolution Imaging

Fluorescence microscopy is an important technique for the observation of living cells. It allows imaging of specific proteins with high contrast and sensitivity. Since antibodies and many organic dyes are cell-impermeable, labeling of a protein of interest in living cells is most often achieved by genetically fusing it to a fluorescent protein.

The resolution of conventional fluorescence microscopy is limited by diffraction to

$$d = \frac{\lambda}{2n \cdot \sin(\alpha)}$$

in the focal plane where λ denotes the wavelength of the light, n the refractive index of the medium between objective lens and coverslip, and α the semi-aperture angle of the objective lens. Therefore, the best resolution that can be achieved with light in the visible range is ~200 nm. This is not sufficient for many applications since various cellular structures are considerably smaller. Several methods have been developed that overcome the diffraction limit and allow imaging at significantly higher resolution. The first concept for far-field superresolution imaging is STED microscopy that was described in 1994 [45]. All techniques for superresolution imaging temporally separate the emission of molecules lying closely together by switching a subset of the fluorophores into a dark (i.e., non-fluorescent) state. Hence, molecules lying closer together than the diffraction limit can be resolved by imaging them sequentially. The different techniques for superresolution imaging can be divided into two major groups, scanning techniques including STED and RESOLFT microscopy and stochastic methods such as PALM (photoactivated localization microscopy) and STORM (stochastic optical reconstruction microscopy).

The stochastic approaches use photoactivatable dyes that are randomly switched on throughout the sample [46-48]. By using low light intensities for photoactivation, the distance between emitting fluorophores can be kept above the diffraction limit so that they can be easily separated. Since the individual fluorophores typically emit several hundreds to thousands of photons per switching cycle, depending on the combination of dye and imaging buffer [49], they can be localized with a precision greater than the diffraction limit. The achieved localization precision is approximately proportional to $\frac{1}{\sqrt{N}}$, with N being the number of recorded photons [50]. After spontaneous off-switching or photobleaching (i.e., the irreversible destruction of the fluorophore by light), the next subset of fluorophores is recorded.

The second approach uses selective deactivation of fluorescence from the outer regions of a diffraction-limited excited area. An image is obtained by scanning over the region of interest. Reduction of the spot size beyond the diffraction limit can be achieved with a second, typically donut-shaped laser beam, which brings the fluorophores in the outer regions of the spot back to a dark state (Figure 8b). STED microscopy uses stimulated emission to drive the transition from the excited state S_1 of the fluorophore (the fluorescent on-state) into its ground state S_0 (the fluorescent off-state) (Figure 8a), thereby preventing emission of fluorescence in this region [45, 51]. Stimulated emission has to occur before spontaneous emission of fluorescence. Since the lifetime of S_1 is usually only a few nanoseconds, high STED intensities are required to effectively suppress the fluorescence. The resolution of a STED microscope is given by

$$d = \frac{\lambda}{2n \cdot \sin(\alpha) \sqrt{1 + \frac{I}{I_S}}}$$

with I denoting the intensity of the STED beam and $I_S = (\sigma\tau)^{-1}$ the intensity at which the population of the excited state has been depleted to $\frac{1}{e}$ [52, 53]. I_S depends on the cross-section σ for stimulated emission and the lifetime τ of S_1. By increasing the STED power so that $I \gg I_S$, $d \to 0$, i.e. there is no principal limit for resolution down to the size of individual fluorophores or even below. The best resolution that has been achieved so far is 2.4 nm in non-biological [54] and 20 nm in biological samples [55]. A different approach to obtain a high $\frac{I}{I_S}$ with lower light intensities is to decrease I_S. Since $I_S \propto \tau^{-1}$, this can be achieved by using a fluorescent state with a longer lifetime. This is the basis for RESOLFT microscopy with RSFPs which can be switched between a fluorescent and a non-fluorescent conformation by light

[56]. Since the lifetime of these conformations is $\gg 1\ \mu s$, the intensity required for off-switching of fluorescence in RESOLFT is several orders of magnitude lower than for STED microscopy.

(a)   (b)
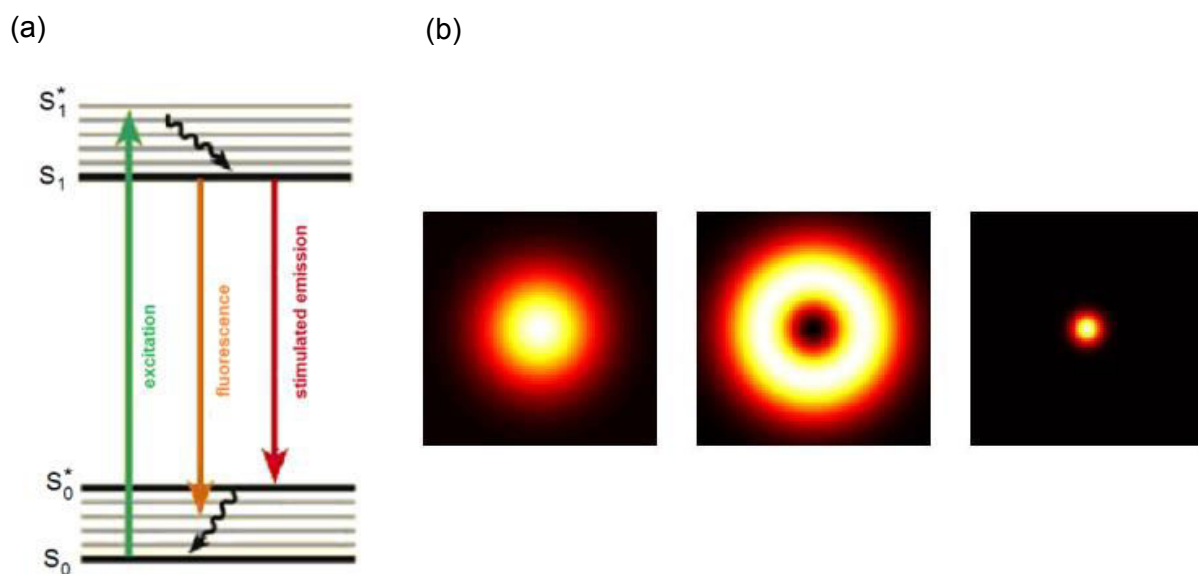
Figure 8: Principles of STED microscopy

(a) (from [57]) Jablonski diagram of a fluorophore. After excitation (green) and fast internal conversion into the excited state S_1, the molecule can return into the ground state by emission of fluorescence (orange), stimulated emission (red), or non-radiative processes (not shown).

(b) (from [58]) Size of the excited spot before (left) and after (right) application of a superimposed donut-shaped STED beam (middle)

Bioluminescence Imaging

Since luciferases, like fluorescent proteins, can be expressed in different cell types, bioluminescence can be used for live cell imaging. Bioluminescence imaging has several advantages but also some drawbacks compared to fluorescence microscopy. The major disadvantage is its very low brightness, often requiring long exposure times. Furthermore, most of the commonly used luciferases exhibit several drawbacks resulting from the need to add the luciferin. These substances are often toxic, poorly soluble and cell-permeable, and must be applied repeatedly to maintain the bioluminescence reaction [59, 60]. Moreover, coelenterazine, the luciferin of *Renilla* and *Gaussia* luciferase, is oxidized non-enzymatically in solution, thereby producing bioluminescence background. Bacterial luciferase is the only exception that does not require addition of an exogenous luciferin since it uses reduced FMN as luciferin which is abundant in all cells. This feature enables long-term measurements

without the need for repeated luciferin addition. Its brightness, however, is several orders of magnitude lower compared to other luciferases [61].

On the other hand, bioluminescence imaging offers several benefits. No excitation light source and filters are required, simplifying the optical system. In addition, no phototoxicity and bleaching occur, allowing imaging of cells over days or even weeks. The bioluminescence background of living tissue is extremely low [59, 62] whereas autofluorescence from cellular molecules such as flavins can lead to significant background in fluorescence measurements. Therefore, detection of bioluminescence is often more sensitive than fluorescence despite its low signal [59, 61]. Another feature of bioluminescence is its dependence on metabolic energy. Therefore, only live and healthy cells are imaged, preventing wrong conclusions from the observation of severely damaged or dead cells.

Different applications of bioluminescence imaging have been demonstrated. For example, bioluminescence has been used to study light-sensitive tissues such as the retina [63] and circadian gene expression [64, 65]. Furthermore, it was applied to observe bacterial infections in fish [66] and growth of tumors in mice [60, 67].

Despite the low technical complexity of a bioluminescence microscope, several issues need to be taken into account for imaging. Due to the low light levels of bioluminescence, as much light from the sample as possible must be detected. Therefore, high numerical objective lenses should be used and the number of optical elements in the light path must be kept as low as possible. In addition, all optical elements should be chosen for optimal performance in the spectral range of bioluminescence light. By using low magnification lenses, the emitted light is distributed over fewer pixels on the detector, resulting in an increased signal-to-noise ratio (SNR), but at the expense of spatial resolution. Furthermore, the detection efficiency of the camera should be as high as possible. Conventional CCD cameras, Intensified CCDs (ICCDs) and Electron-Multiplying CCDs (EMCCDs) are most often used for bioluminescence imaging due to their high sensitivity [59]. On the other hand, the background signal has to be kept low to achieve an optimal SNR. Consequently, stray light from the environment must be eliminated. The second source of background is the camera itself. There are two different sources of camera noise: readout noise which is produced during the readout process, and dark noise due to fluctuations of dark current that increases with exposure time. Dark noise can be reduced by cooling the camera to -90 or -100 °C whereas the effect of readout noise can be reduced by the usage of an EMCCD instead of a normal CCD camera and by slower readout and longer exposure times [59].

Although a setup for bioluminescence imaging can be self-built, a microscope particularly designed for long-term bioluminescence measurements has become commercially available [68]. In addition to shielding sample and optics from external light, it allows regulation of temperature, humidity, and gas flow to keep the cultured cells under optimal conditions for extended observation times [68].

Objective of this Work

RESOLFT microscopy with reversibly switchable fluorescent proteins enables sub-diffraction imaging of living cells with relatively low light intensities. It requires proteins that are bright, can undergo multiple switching cycles, and exhibit fast switching to enhance the speed of imaging. The RSFPs existing so far have been engineered from GFP and related proteins which are not ideal for all purposes due to their relatively large size, oxygen-dependence, and pH sensitivity. Therefore, the development of new RSFPs with different properties is expected to extend the scope of application of RESOLFT microscopy. The LOV domain from the bacterial photoreceptor YtvA has been shown to be useful for PALM [36], but its low brightness and low extent of on-switching prevent its application for RESOLFT microscopy. Therefore, the first objective of this thesis was the improvement of switching and brightness of YtvA-LOV for other types of superresolution imaging (see chapter I).

Microscopy can be performed at even lower light levels using bioluminescence which does not require excitation light. However, its low signal and the need for exogenous luciferin addition limit its use for imaging. Hence, brighter luciferases with autonomous bioluminescence are desirable. The second objective of this work was the development of a brighter version of bacterial luciferase that does not require an exogenous luciferin (see chapter II).

Chapter I: Novel reversibly switchable fluorescent proteins engineered from the bacterial photoreceptor YtvA

Carola Gregor[1], Sven C. Sidenstein[1], Martin Andresen[1], Johann G. Danzl[1], Stefan W. Hell[1]

[1] Department of NanoBiophotonics, Max Planck Institute for Biophysical Chemistry, Am Fassberg 11, 37077 Göttingen, Germany

Preface

The aim of this study was the generation of a new reversibly switchable fluorescent protein (RSFP) from the LOV domain of the photoreceptor protein YtvA from *Bacillus subtilis*. The work was supervised by Prof. Dr. Stefan Hell. Wild-type YtvA-LOV in pET28a was provided by Prof. Dr. Wolfgang Gärtner (Max Planck Institute for Chemical Energy Conversion, Mülheim). The STED/RESOLFT microscope was built and maintained by Dr. Sven Sidenstein and Dr. Johann Danzl. Dr. Martin Andresen maintained and aided with the screening systems. STED and RESOLFT imaging was performed by me and Dr. Sven Sidenstein. Absorption and emission spectra were taken by Kurt Müller. Mutagenesis, screening, cloning, sample preparation, and all other experiments described were performed by me. I conceptualized and wrote this manuscript.

Chapter I: Novel reversibly switchable fluorescent proteins engineered from the bacterial photoreceptor YtvA

Carola Gregor[1], Sven C. Sidenstein[1], Martin Andresen[1], Johann G. Danzl[1], Stefan W. Hell[1]

[1] Department of NanoBiophotonics, Max Planck Institute for Biophysical Chemistry, Am Fassberg 11, 37077 Göttingen, Germany

Abstract

The reversibly switchable fluorescent proteins (RSFPs) commonly used for RESOLFT microscopy are all developed from fluorescent proteins of the GFP superfamily [69-75]. These proteins are bright and photostable, but exhibit several drawbacks such as relatively large size, oxygen-dependence, sensitivity to low pH, and limited switching speed. Therefore, RSFPs from other origins with improved properties are needed. Here, we report the development of two RSFPs based on the LOV domain of the photoreceptor protein YtvA from *Bacillus subtilis*. The first variant, rsLOV1, can be used for RESOLFT microscopy, whereas rsLOV2 proved useful for STED imaging of living cells with a resolution of down to 40–50 nm. In addition to their smaller size compared to GFP-related proteins (17 kDa instead of 27 kDa), rsLOV1 and rsLOV2 exhibit ultrafast switching kinetics and switch on and off 3 times faster than rsEGFP2, the fastest switching RSFP published so far. Therefore, LOV domain-based RSFPs may prove useful for applications where the switching speed of GFP-based proteins is limiting.

Introduction

The resolution of conventional fluorescence microscopes is limited by diffraction to $\frac{\lambda}{2 \cdot NA}$, with λ denoting the wavelength and NA the numerical aperture of the objective lens. Therefore, structures residing closer together than ~200 nm cannot be discerned using light in the visible range. However, several methods breaking the diffraction limit have been developed, including STED and RESOLFT microscopy with reversibly switchable fluorescent proteins (RSFPs), that allow imaging of living cells with enhanced resolution. STED microscopy uses stimulated emission to silence fluorophores located in the outer regions of a diffraction-limited excitation spot, thereby decreasing the area from which fluorescence is emitted. Since

stimulated emission has to occur before spontaneous emission of fluorescence, relatively high STED intensities are required as the lifetime of the excited state is typically in the range of only a few nanoseconds. The light intensity required to switch molecules into a dark state can be decreased if a long-lived fluorescent on-state and non-fluorescent off-state are used. This is the basis for RESOLFT microscopy that uses the switching of fluorescent proteins between two different conformations, one of which is non-fluorescent [56].

The speed of imaging in RESOLFT microscopy is limited by the switching kinetics of the RSFP. This can be a problem for the observation of quickly moving structures in living cells. For this purpose, GFP-related RSFPs have been developed that are optimized for fast switching [73, 74], achieving pixel dwell times during imaging of down to 75 µs [73, 76]. All commonly used RSFPs are derived from GFP-related proteins and share the same β barrel structure with a tripeptide forming the chromophore at the center. Therefore, they share several features that limit their applicability as fluorescent reporter proteins. First, their relatively large size of 27 kDa can affect the function of fusion proteins and therefore lead to the observation of artifacts. Second, GFP fluorescence is strongly quenched at low pH, impeding imaging of acidic organelles such as lysosomes. Third, GFP fluorescence is dependent on oxygen for chromophore maturation and can therefore not be used under anaerobic conditions. FMN (flavin mononucleotide)-binding fluorescent proteins (FbFPs) overcome all these limitations. They are small (12–19 kDa [35]) and their fluorescence is oxygen-independent and less sensitive to low pH [1, 30]. FbFPs were engineered from different LOV (light-oxygen-voltage sensing) domains [30-33] that non-covalently bind FMN, a cofactor that is abundant in all cell types. Upon absorption of blue light, LOV domains undergo a photocycle that leads to formation of a covalent bond between the FMN and a cysteine residue of the protein, thereby switching it into a non-fluorescent state. After seconds to hours, the photoadduct decays back into the non-covalently bound, fluorescent state. To make LOV domains constitutively fluorescent with emission in the green range, their photoactive cysteine residue was mutated into alanine. In addition, their brightness and photostability were further improved by mutagenesis [31, 32]. On the other hand, their inherent photoswitching makes LOV domains interesting for superresolution microscopy. This has been demonstrated for the first time with the LOV domain from the photoreceptor protein YtvA from *Bacillus subtilis* in PALM imaging [36]. In this study, the wild-type LOV domain was used that has a relatively weak fluorescence and switches back into the fluorescent state under UV light to less than 10 % [36]. This impedes its use for RESOLFT microscopy where multiple switching cycles have to be performed. We aimed at improving switching and brightness of

21

YtvA-LOV by site-directed and error-prone mutagenesis to enable RESOLFT imaging and demonstrate that the effective brightness could be increased ~10-fold compared to the wild-type protein. In addition, we generated another variant with an even ~2-fold further increased fluorescence that was used for STED microscopy.

Results

To improve the brightness of YtvA-LOV upon 488 nm excitation after repeated on- and off-switching with 405 and 488 nm light, respectively, multiple rounds of site-directed and error-prone mutagenesis were performed. Colonies of *E. coli* DH5α cells expressing YtvA-LOV mutants from the vector pGEX-6P-1 were grown at 37 °C and screened for improved brightness after repeated switching with an automated microscope. Multiple mutations were identified that contributed to enhanced brightness by improved on-switching and possibly also by better expression and folding at 37 °C. Two final variants, named rsLOV1 and rsLOV2 (reversibly switchable LOV1 and 2), were obtained that contain the mutations indicated in Figure 9. rsLOV1 exhibits similar brightness as the wild-type LOV domain (LOV wt) in the first switching cycle, measured as the amplitude of off-switching. However, upon irradiation with UV light (405 nm), 57 % of the initial brightness is recovered, compared to ~5 % for LOV wt under our screening conditions (Figure 10). This corresponds to a ~10-fold increase in reversibly switchable fluorescence required for RESOLFT imaging. The switching background of rsLOV1 is less than 3 %, indicating an almost complete off-switching with 488 nm light. rsLOV2 exhibits a brightness ~2 times higher than LOV wt in the first cycle and shows an even better on-switching to 78 % of the initial value, increasing the overall effective brightness ~30-fold compared to the wild-type protein. However, the switching background of rsLOV2 increases after repeated switching (Figure 10), an undesirable feature for RESOLFT applications.

```
LOV wt      MASFQSFGIPGQLEVIKKALDHVRVGVVITDPALEDNPIVYVNQGFVQMTGYETEEILGK
rsLOV1      MTRFQSFGISGQLEVIKNALDHLRVGVVITDPAREDNPIVYVNQGFVQMTGYEAEEILGK
rsLOV2      MTRFQSFGISGQLEVIKNALDHLRVGVVITDPAREDNPVVYVNNGFVQMTGYEAEEILGK
            *:  ****** *******:****:********** ****:****:**********:******


LOV wt      NCRFLQGKHTDPAEVDNIRTALQNKEPVTVQIQNYKKDGTMFWNELNIDPMEIEDKTYFV
rsLOV1      NCRILQGEHTDPAEVDIIRTALQNKEPVTVQILNYRKDGTMFWNLLHIVPIVIEGKTYFV
rsLOV2      SCRILQGEHTDPAEVDIIRTALQNKEPVTVQILNYRKDGTMFWNLLHIVPIVIEGKTYFV
            .**:***:******** **************** **:******** *.* *: ** *****


LOV wt      GIQNDITKQKEYEKLLEDSLTEITAL
rsLOV1      GNQNDITKQKEYEKLLERPHRG----
rsLOV2      GNQNDITKQKEYEKLLERPHRG----
            * *  *************
```

Figure 9: Sequence alignment of YtvA-LOV wt (aa 1–146), rsLOV1, and rsLOV2

rsLOV1 and rsLOV2 consist of the first 137 amino acids of YtvA with the indicated mutations and have a deviating C-terminal extension.
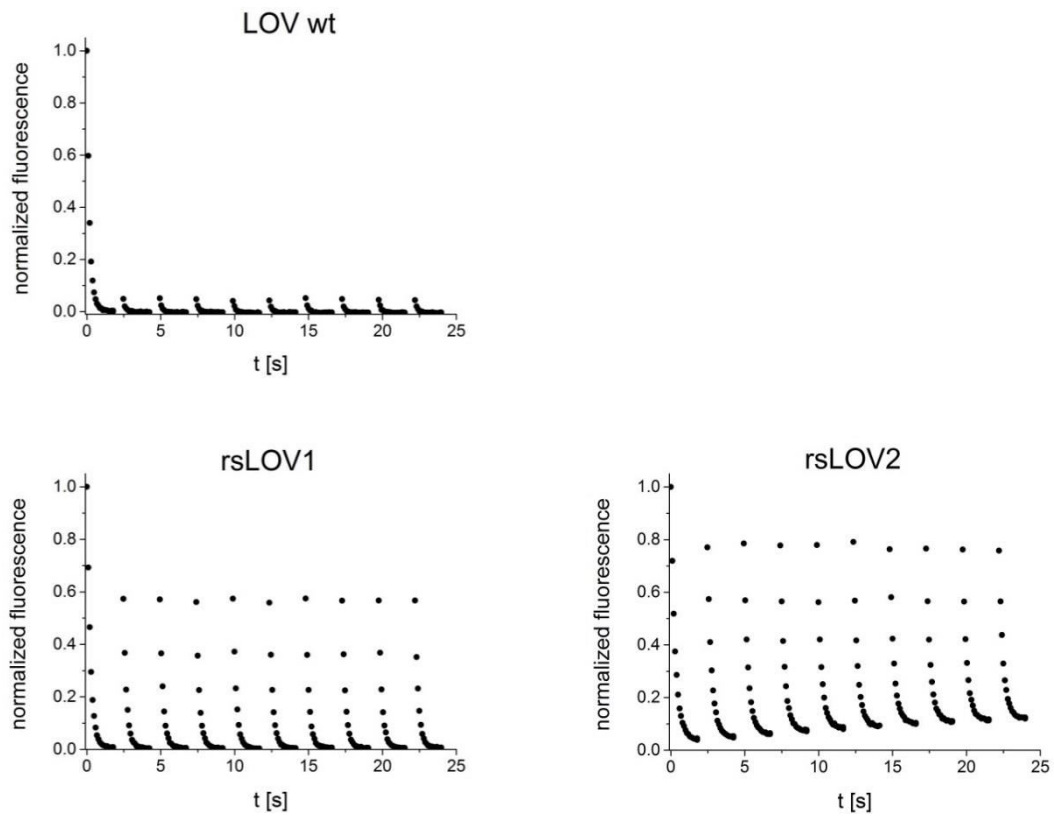

Figure 10: Switching of YtvA-LOV wt, rsLOV1, and rsLOV2 under low-power screening conditions

Purified proteins in solution were switched off with 488 nm light (~2 W·cm^{-2}) for 2 s and switched on with 405 nm light (~5 W·cm^{-2}) for 0.5 s. For better clarity, only off-switching is shown. The fluorescence signal is normalized to the initial value.

To determine the photostability of rsLOV1 and rsLOV2 upon repeated switching, we measured 500 switching cycles under the low power conditions used for screening. Screening was performed under low-power conditions (few W·cm^{-2}) because of the poor signal from *E. coli* colonies. rsLOV1 retains 72 % of its brightness after 500 switching cycles whereas rsLOV2 is bleached to 27 % of its initial value (Figure 11). Under high-power excitation comparable to RESOLFT imaging conditions, however, rsLOV1 and rsLOV2 lose 50 % of their brightness within the first 10 and 3 switching cycles, respectively. This loss of signal is reversible and is almost fully reconstituted after a break of 1 min (Figure 12), possibly indicating the transition into a long-lived triplet state. Similar reversible photobleaching has also been described for the LOV domain-based fluorescent protein iLOV [31] where the photocycle is abolished.
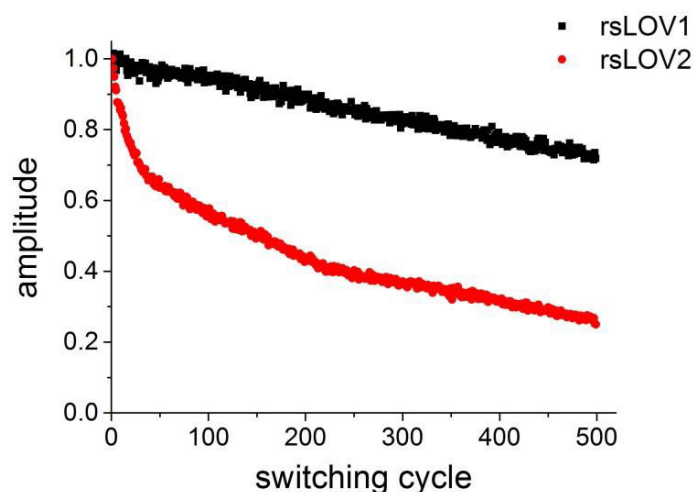
Figure 11: Brightness of rsLOV1 and rsLOV2 after 500 switching cycles under low power conditions.
Purified proteins in solution were switched off with 488 nm light for 2 s (~2 W·cm^{-2}) and switched on with 405 nm light (~5 W·cm^{-2}) for 0.5 s 500 times. Off-switching curves were fitted with a single exponential decay function. The normalized amplitudes of the fits are displayed. The first switching cycle was omitted.
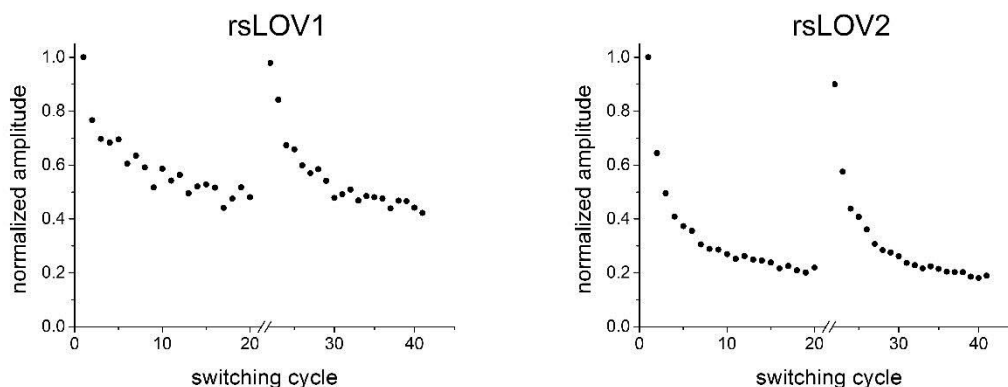
Figure 12: Fast "bleaching" of rsLOV1 and rsLOV2 under high-power conditions is reversible.
40 switching cycles of rsLOV1 and rsLOV2 were recorded under high-power conditions (~100 kW·cm^{-2} for 405 nm and ~300 kW·cm^{-2} for 488 nm) with a break of 1 min after the first 20 switching cycles. Normalized off-switching amplitudes fitted with a single exponential function are shown. Measurements were performed in *E. coli* SURE colonies to rule out diffusional effects.

We compared the switching kinetics of rsLOV1 and rsLOV2 as well as the wild-type protein LOV wt to rsEGFP2, the fastest switching RSFP published so far. On- and off-switching were performed at 405 and 488 nm, respectively, with the same powers for all proteins. LOV wt, rsLOV1, and rsLOV2 switch on ~3 times faster than rsEGFP2 (Figure 13). The on-switching time constant of rsLOV1 and rsLOV2 is not significantly affected by mutagenesis. LOV wt switches off 5 times faster than rsEGFP2. Off-switching in rsLOV1 and rsLOV2 is slower, but still faster than rsEGFP2 by a factor of 3 and 1.4, respectively, making them interesting for fast RESOLFT imaging.
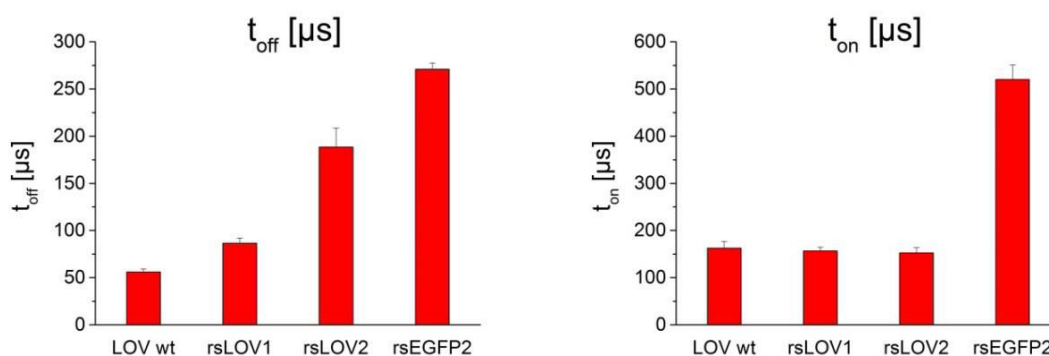

Figure 13: Time constants of on- and off-switching of YtvA-LOV wt, rsLOV1, rsLOV2, and rsEGFP2
Measurements were performed with purified proteins under high-power conditions (~100 kW·cm^{-2} for 405 nm and ~300 kW·cm^{-2} for 488 nm). On- and off-switching curves were fitted with a single exponential function. Error bars represent standard deviation of the mean.

We measured spectra of purified GST-tagged LOV wt, rsLOV1, and rsLOV2 (Figure 14). The spectra of rsLOV1 and rsLOV2 are similar to the wild-type protein with absorption and fluorescence emission maxima of ~450 and 498 nm, respectively. Extinction coefficients ε were calculated from the absorption at 450 nm (Table 1), assuming that the proteins are fully saturated with FMN. Therefore, the given values represent only a lower limit for ε. Quantum yields were determined using FMN as a reference (ϕ_{fl} = 0.246 [34]). Our data indicate that the extinction coefficients of rsLOV1 and rsLOV2 are not significantly altered by mutagenesis. In addition, the quantum yield of rsLOV1 is identical to that of LOV wt, demonstrating that its improved brightness under imaging conditions is solely due to improved on-switching. rsLOV2 exhibits a quantum yield almost 2 times higher than LOV wt, consistent with the amplitudes measured during the first cycle of off-switching (data not shown). These data demonstrate that the brightness of rsLOV1 and rsLOV2 is still low compared to EGFP (6 % and 11 % of EGFP for rsLOV1 and rsLOV2, respectively, as calculated from the product of extinction coefficient and quantum yield, assuming ε = 55,000 $M^{-1} \cdot cm^{-1}$ and ϕ_{fl} = 0.60 for EGFP [77, 78]).

(a) (b)
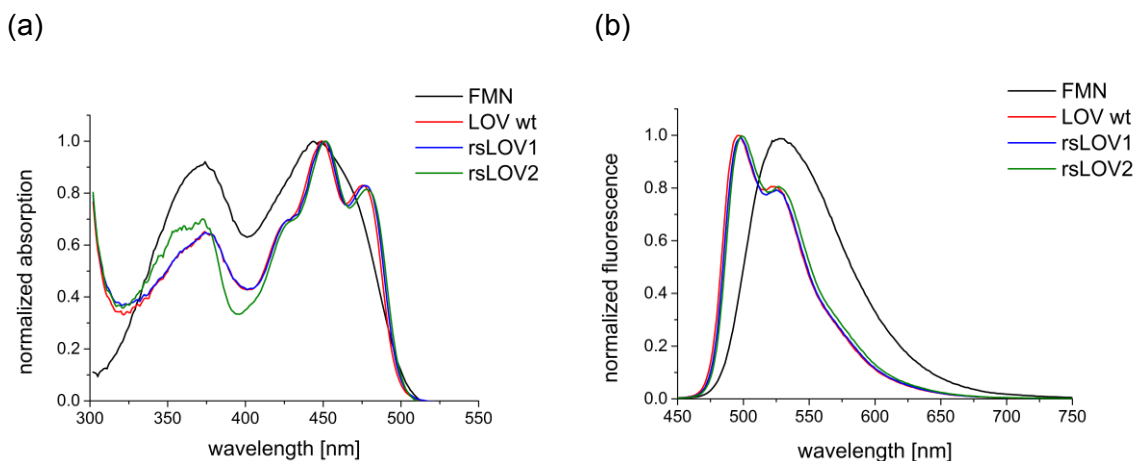
Figure 14: Absorption and fluorescence emission spectra of FMN, LOV wt, rsLOV1, and rsLOV2

(a) Normalized absorption spectra of FMN, LOV wt, rsLOV1, and rsLOV2

(b) Normalized fluorescence emission spectra of FMN, LOV wt, rsLOV1, and rsLOV2 excited at 440 nm

|	$\varepsilon_{450\ nm}$ [$M^{-1} \cdot cm^{-1}$]	ϕ_{fl}
LOV wt	12,700	0.17
rsLOV1	10,900	0.17
rsLOV2	11,400	0.31

Table 1: Extinction coefficients at 450 nm and fluorescence quantum yields of LOV wt, rsLOV1, and rsLOV2

Wild-type YtvA-LOV (aa 25–126) has been reported to dimerize, whereas dimerization is prevented in full-length YtvA [26]. We observed that GST-tagged YtvA-LOV (aa 1–146), rsLOV1, and rsLOV2 migrate mostly as monomers on semi-native gels (Figure 15). To test the behavior of rsLOV2 in mammalian cells, we expressed a fusion protein of rsLOV2 and histone H2B that requires a monomeric tag for proper localization (Figure 16). We observed that localization of rsLOV2-H2B is not impaired, indicating that rsLOV2 is predominantly monomeric under cellular conditions. rsLOV2 was also used for labeling of other cellular structures (Figure 16), demonstrating its use as a protein tag in living cells. Its brightness, however, is relatively low. Therefore, autofluorescence from lysosomes around the nucleus is clearly visible in some cells.
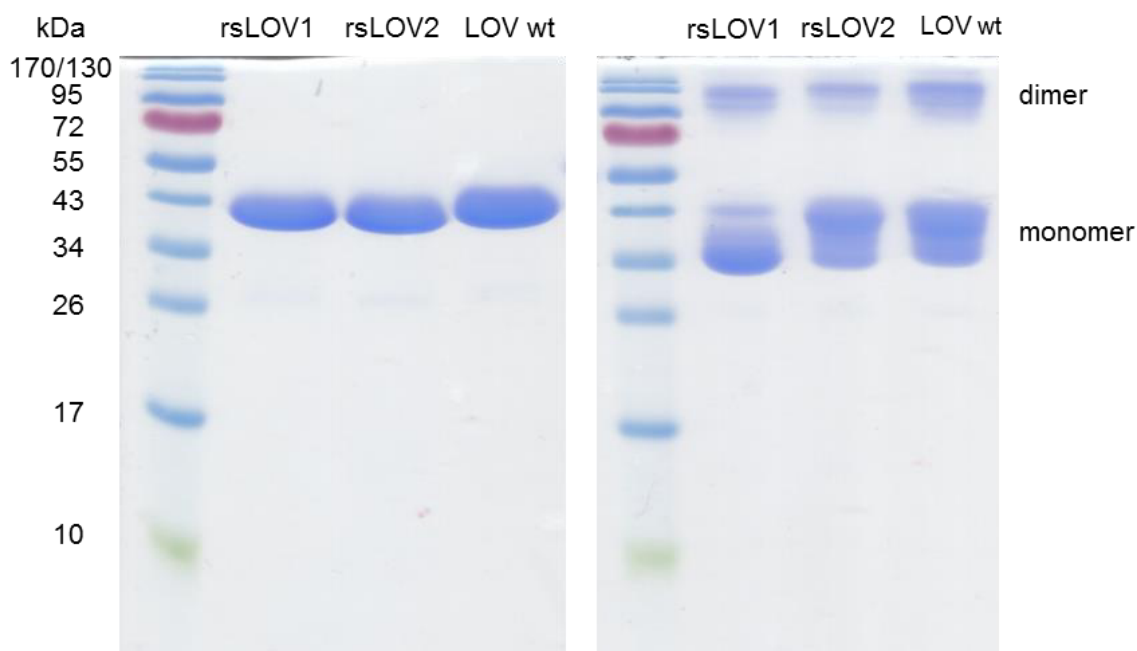
Figure 15: SDS- and seminative gel of GST-tagged rsLOV1, rsLOV2, and LOV wt

Proteins were purified from *E. coli* SURE cells. 15 µg of each protein was applied to a denaturing gel containing 0.1 % SDS (left) or a seminative gel (right). Gels were stained with Coomassie Brilliant Blue.
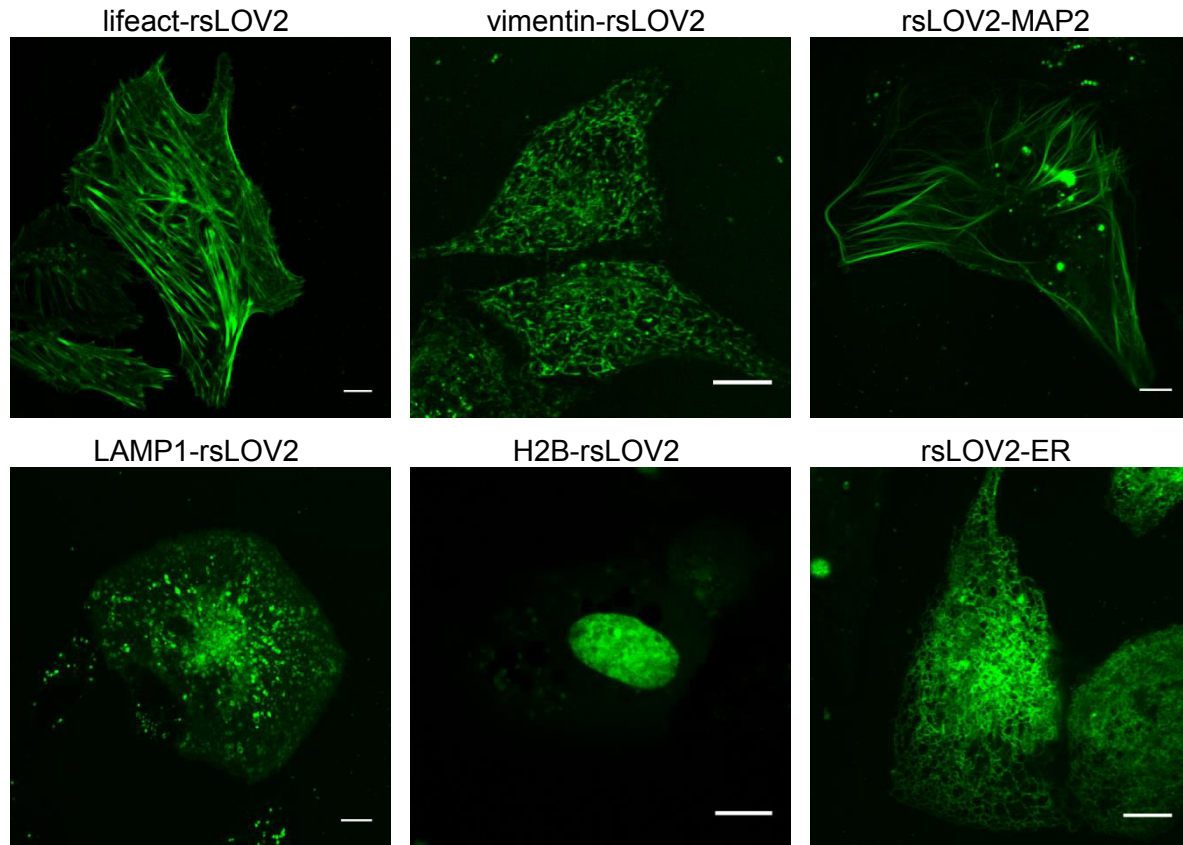
Figure 16: Expression of different fusion proteins of rsLOV2 in living cells

Lifeact-rsLOV2, rsLOV2-MAP2, LAMP1-rsLOV2, histone H2B-rsLOV2, and rsLOV2-KDEL for targeting into the endoplasmic reticulum were expressed in CV-1 cells. Vimentin-rsLOV2 was expressed in HeLa cells. Images of living cells were taken with a confocal Leica SP8 microscope with simultaneous excitation at 405 and 488 nm light. Scale bar, 10 µm

The fluorescence of LOV domains from different origin has been found to be insensitive to changes in pH over a broad range [1]. This makes LOV domains superior for imaging at low pH where GFP fluorescence is strongly quenched. To test if this feature is preserved in rsLOV1 and rsLOV2, CV-1 cells expressing lifeact-EGFP, lifeact-rsLOV1, and lifeact-rsLOV2 were permeabilized with nigericin and imaged in citric acid/phosphate buffer at pH 7 and 4 (Figure 17). As expected, EGFP fluorescence is strongly quenched at low pH whereas fluorescence from rsLOV1 and rsLOV2 is largely preserved at pH 4.
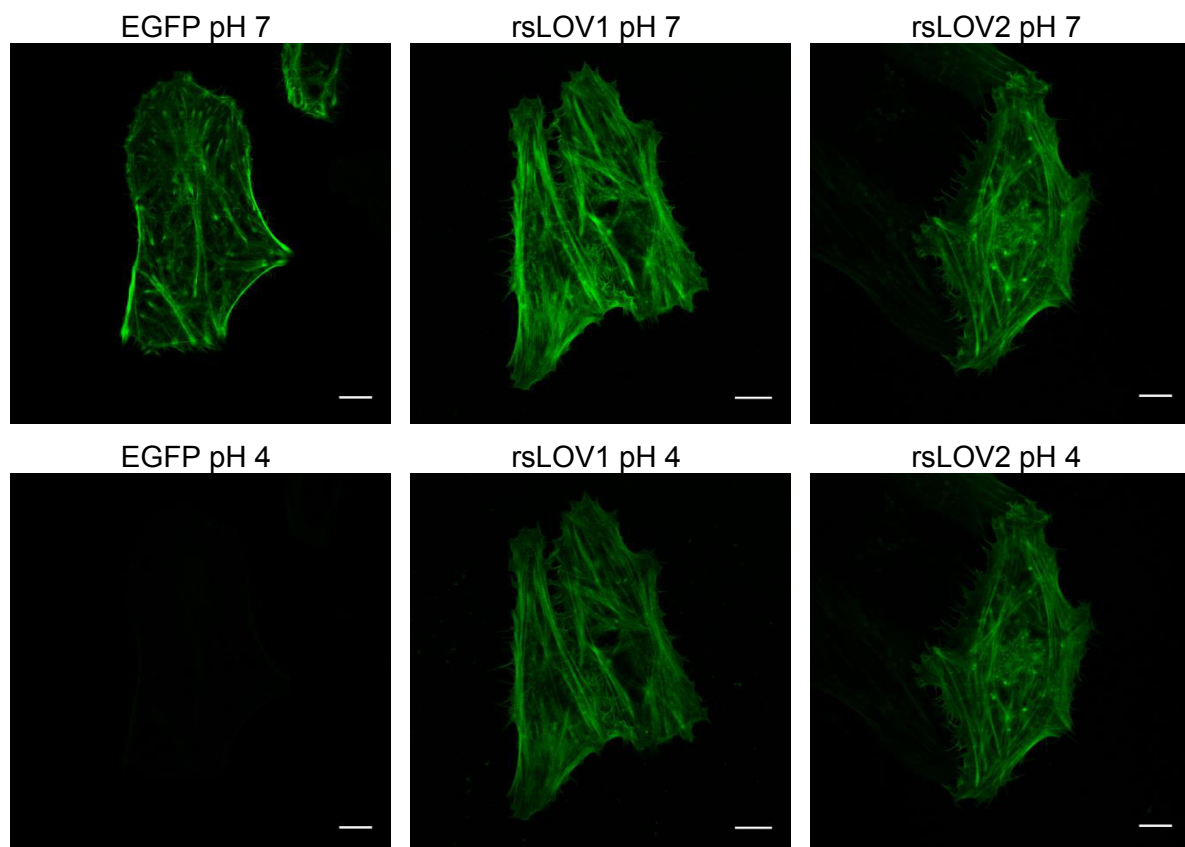
Figure 17: Fluorescence of lifeact-EGFP, -rsLOV1, and -rsLOV2 at pH 7 and 4.

CV-1 cells expressing lifeact-EGFP, lifeact-rsLOV1, and lifeact-rsLOV2 were permeabilized with 1 µM nigericin in citric acid/phosphate buffer of pH 7 and 4. Images were taken with a confocal Leica SP8 microscope. Scale bar, 10 µm

We used rsLOV1 for RESOLFT imaging of actin in living CV-1 cells (Figure 18). For each pixel, the proteins were switched on with 405 nm light for 10 µs, switched off with a 488 nm donut for 200 µs, and read out with a confocal 488 nm beam for 5 µs. To gain sufficient signal, 20 scans per line were accumulated. A resolution of ~60–65 nm was achieved. The resolution seems to be limited by the low brightness of rsLOV1, as thinner and therefore darker filaments do not provide sufficient signal above background. Interestingly, the second protein rsLOV2 proved to be useful for STED imaging (Figure 19). Apart from the reversible photobleaching, the protein seems to be very photostable even at high STED intensities. We observed that bleaching is reduced when omitting the 405 nm on-switching pulse and that imaging can be performed with 488 nm excitation and simultaneous 618 nm STED only. Lines were scanned 3 times with a pixel dwell time of 200 µs. A resolution of down to 40–50 nm was achieved.
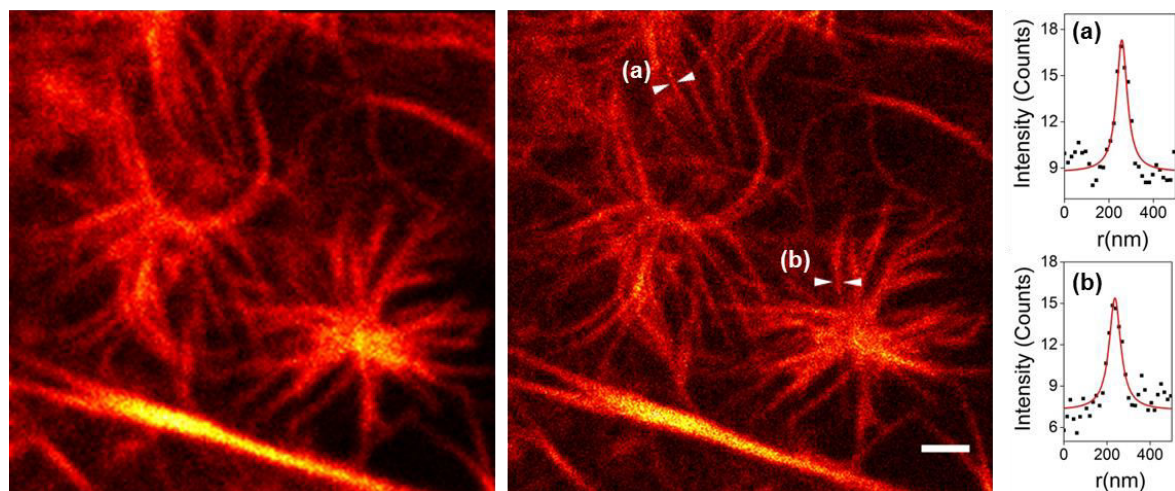
Figure 18: Confocal (left) and RESOLFT image (right) of lifeact-rsLOV1

Living CV-1 cells expressing lifeact-rsLOV1 were imaged with the following pulse sequence: 10 µs activation (405 nm confocal), 1 µs break, 200 µs deactivation (488 nm donut), 1 µs break, 5 µs readout (488 nm confocal). The signal from 20 scans per line was accumulated. Images represent raw data. Line Profiles were fitted with a Lorentzian Function. FWHM values of (a) and (b) are 58 nm and 66 nm, respectively. Scale bar, 1 µm
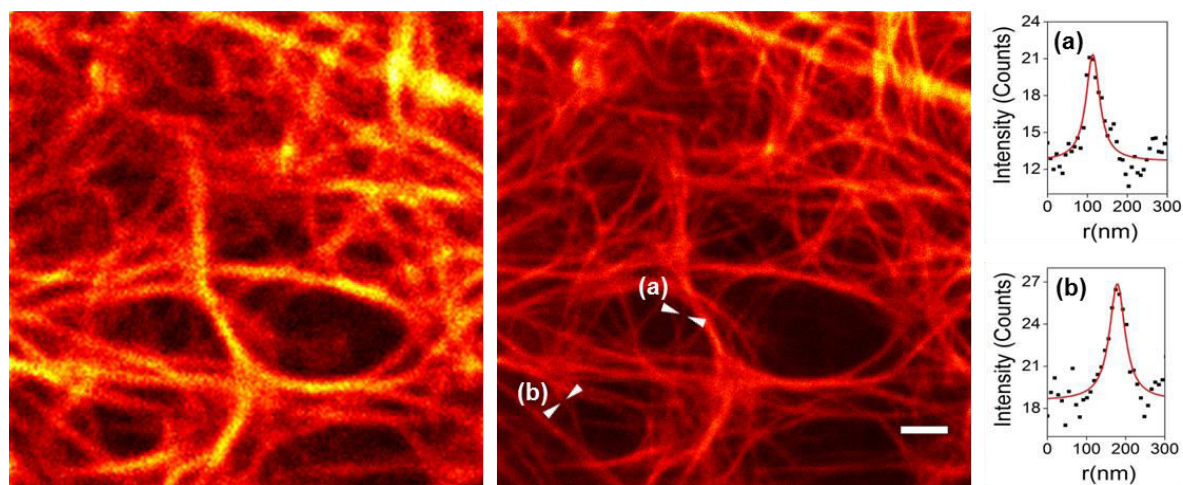
Figure 19: Confocal (left) and STED image (right) of lifeact-rsLOV2

Living CV-1 cells expressing lifeact-rsLOV2 were imaged with 488 nm excitation (pulsed) and 618 nm STED (pulsed) with a pixel dwell time of 200 µs. The signal from 3 scans per line was accumulated. Images represent raw data. Line Profiles were fitted with a Lorentzian Function. FWHM values of (a) and (b) are 41 nm and 48 nm, respectively. Scale bar, 1 µm

Discussion

The potential of wild-type YtvA-LOV for PALM imaging has already been outlined [36], but its low brightness in combination with inefficient on-switching hinders its use for RESOLFT microscopy. In this work, it was demonstrated that the extent of on-switching of YtvA-LOV by 405 nm light can be improved 10-fold by mutagenesis, resulting in the new protein rsLOV1 that could be used for RESOLFT imaging of living cells with a resolution of down to ~60–65 nm. An interesting feature of rsLOV1 is its ultrafast on- and off-switching, pointing out its potential for faster RESOLFT imaging than it has been achieved with GFP-related RSFPs so far. Yet, the low number of photons per switching cycle of rsLOV1 required repeated scanning of the sample to gain sufficient signal, thereby reducing the speed of imaging. Hence, further improvements in the brightness of rsLOV1 would be beneficial. This could be achieved either by further changes in the protein sequence or by exchanging its cofactor FMN against flavins with higher extinction coefficients and quantum yields, as it has been done *in vitro* [12, 79]. However, the modified cofactor would need to be incorporated into the protein *in vivo* and is likely to influence the switching behavior. Therefore, further mutagenesis and screening in the presence of the exchanged cofactor might be necessary for improving the performance further.

A second variant, rsLOV2, is brighter than rsLOV1, but displays a significant switching background that hinders its application for RESOLFT imaging. It was demonstrated, however, that rsLOV2 can be used for STED imaging with a resolution of down to ~40–50 nm despite its faster apparent photobleaching under low-power screening conditions. Interestingly, rsLOV2 exhibited very little photobleaching even at high STED intensities at 618 nm (38 mW in the back aperture) when excited at 488 nm. Yet, previous or simultaneous irradiation with 405 nm led to a fast decrease in fluorescence even during confocal imaging. Surprisingly, STED imaging with 488 nm excitation without previous on-switching turned out to be superior for imaging. Possible explanations for this observation are either on-switching by two-photon absorption from the STED beam or imaging of the switching background only with less protein accumulating in long-lived dark states than by excitation with 405 nm. By specific optimization of FbFPs for STED, it might be possible to generate even brighter and more photostable proteins that would supplement the toolbox of fluorescent proteins for superresolution imaging of living cells.

Materials and Methods

Mutagenesis and Screening

The LOV domain of YtvA including the C-terminal linker (aa 1–146) was cloned into the vector pGEX-6P-1 between the BamHI and SalI restriction sites. Error-prone PCRs were performed with the primers TTAGTCGGATCCATGGCTAGTTTTCAATCA and TTAGTCGTCGACTTAAAGTGCAGTAATTTC with 25 PCR cycles and $MnCl_2$ concentrations ranging from 100 to 300 µM. Screening was performed with the expression vector pGEX-6P-1 in *E. coli* DH5α cells. Cells were grown on LB agar plates over night at 37 °C and screened at room temperature. Screening was performed with an automated microscope under low-power conditions with 405 nm (~2 W·cm^{-2}) and 488 nm (~5 W·cm^{-2}) for on- and off-switching, respectively.

Protein purification and characterization

GST-tagged LOV wt, rsLOV1, rsLOV2, and EGFP were expressed from the vector pGEX-6P-1 in *E. coli* SURE cells. Cells were grown at 37 °C to an OD_{600} between 0.5 and 0.6 and induced with 1 mM IPTG (AppliChem) over night at 30 °C. Cells were lysed in B-PER solution (Thermo Scientific) and purified by affinity chromatography with glutathione spin columns (Thermo Scientific) according to the instructions of the manufacturer. The eluted protein was ultrafiltrated against 150 mM NaCl, 50 mM Tris-HCl, pH 8.0. All measurements with purified proteins were performed in this buffer. Protein concentration was determined by Bradford assay. Fluorescence measurements under low-power conditions were performed with approximate intensities of 5 W·cm^{-2} for 405 nm and 2 W·cm^{-2} for 488 nm. Intensities under high-power conditions were approximately 100 kW·cm^{-2} for 405 nm and 300 kW·cm^{-2} for 488 nm. Gel electrophoresis was performed with 15 % acrylamide gels containing 0.1 % SDS. For denaturing gels, samples were boiled for 2 min at 99 °C in a loading buffer containing 100 mM DTT and 2 % (w/v) SDS. For seminative gels, samples were applied to the gel in a loading buffer without DTT and SDS without previous heating.

Absorption and fluorescence emission spectra were recorded with a Varian Cary 4000 UV/VIS spectrophotometer and a Varian Cary Eclipse fluorescence spectrophotometer, respectively. Measurements were performed without previous illumination of the proteins in order to keep the proteins in the fluorescent on-state. Extinction coefficients were calculated from the protein concentrations determined by the absorption at 450 nm and Bradford assay assuming that the proteins are fully saturated with FMN. Quantum yields of GST-tagged LOV wt, rsLOV1, and rsLOV2 were determined using FMN (HPLC-purified, purity ≥ 95 %, Sigma-Aldrich) as a reference, assuming a quantum yield for FMN of 0.246 [34]).

Cloning

Codon-optimized versions of rsLOV1 and rsLOV2 for expression in mammalian cells were cloned into into the given vectors with the primers and restriction enzymes indicated in Table 2. Lifeact, MAP2, LAMP1, and H2B were integrated into pcDNA3.1(+) with the following restriction enzymes: lifeact: HindIII / BamHI, MAP2: AscI / NotI, LAMP1: HindIII / BamHI, H2B: NheI / HindIII. Vimentin-rsLOV2 was expressed from the vector pmKate2 where vimentin was integrated between the EcoRI and AgeI restriction sites.

construct	primer	sequence
lifeact	rsLOV BamHI fwd	GTTGATGGATCCACCGGTCGCCACCATGACAAGATTTCAGTCA
	rsLOV NotI rev	TTGATCGCGGCCGCTCAGCCTCTGTGCGGTCTCTC
MAP2	rsLOV NheI fwd	AAGCTGGCTAGCATGACAAGATTTCAGTCA
	rsLOV AscI rev	GATCCTGGCGCGCCGCCTCTGTGCGGTCTCTC
LAMP1	rsLOV EcoRI fwd	GTGGTGGAATTCCATGACAAGATTTCAGTCA
	rsLOV XhoI rev	TCTAGACTCGAGTCAGCCTCTGTGCGGTCTCTC
H2B	rsLOV BamHI fwd	GAATCAGGATCCATGACAAGATTTCAGTCA
	rsLOV XbaI rev	ATCAACTCTAGATCAGCCTCTGTGCGGTCTCTC
vimentin	rsLOV AgeI fwd	GTAGATACCGGTCGCCACCATGACAAGATTTCAGTCA
	rsLOV NotI rev	TTGATCGCGGCCGCTCAGCCTCTGTGCGGTCTCTC

Table 2: Primers used for cloning of lifeact, MAP2, LAMP1, H2B, and vimentin constructs of rsLOV1 and rsLOV2

Mammalian cell culture

CV-1 and HeLa cells were grown in DMEM with 4.5 g/l glucose (Gibco) supplemented with 10 % FBS, 1 mM sodium pyruvate, 100 units/ml penicillin, and 100 µg/ml streptomycin (all Biochrom). Cells were cultured at 37 °C with 5 % CO_2. CV-1 and HeLa cells were transfected with Lipofectamine 2000 (Invitrogen) according to the protocol of the manufacturer and imaged the following day.

Imaging

Confocal images were taken with a Leica SP8 microscope with simultaneous excitation at 405 and 488 nm for rsLOV1 and rsLOV2. EGFP fluorescence was excited at 488 nm. For measurements at

different pH, living CV-1 cells were permeabilized with 1 µM nigericin (Sigma Aldrich) in a citric acid/phosphate buffer of pH 7 or 4 supplemented with 140 mM KCl (Sigma Aldrich).

RESOLFT and STED images were taken with a home-built setup described in [76]. The STED laser was exchanged to a fibre laser with a repetition rate of 40 MHz and a wavelength of 618 nm (MPB Communications Inc.). Following powers were used for RESOLFT imaging (measured in the back aperture): 405 nm activation: 5.1 µW (CW), 488 nm off-switching (donut): 4.8 µW (CW), 488 nm readout (confocal): 4.2 µW (pulsed, repetition rate 40 MHz). Imaging was performed with the following pulse sequence: 10 µs activation (405 nm), 1 µs break, 200 µs deactivation (488 nm donut), 1 µs break, 5 µs readout (488 nm confocal). The signal from 20 scans per line was accumulated. The pixel size was 50 nm for confocal and 30 nm for RESOLFT images. Images represent raw data.

For STED imaging, following powers were used (measured in the back aperture): 488 nm excitation (confocal): 3.0 µW, 618 nm STED (donut): 38 mW (both lasers pulsed, repetition rate 40 MHz). Pixel dwell time was 200 µs. Nanosecond time gating was used. The signal from 3 scans per line was accumulated. The pixel size was 50 nm for confocal and 15 nm for STED images. Images represent raw data.

Data Analysis

To determine switching time constants and amplitudes, switching curves were fitted with Matlab software (MathWorks) using the single exponential function $y = y0 + A \cdot e^{-\frac{t}{\tau}}$ with t denoting the time, y the fluorescence signal, $y0$ the switching background, A the amplitude, and τ the switching time constant.

Resolution of RESOLFT and STED images was determined by the FMWH (full width at half maximum) of line profiles with a width of 5–10 pixels. The signal was fitted with a Lorentzian function $y = y0 + \frac{2 \cdot A}{\pi} \cdot (\frac{w}{4(x - x_C)^2} + w^2)$ with w denoting the FWMH using OriginPro software (OriginLab).

Chapter II: *ilux*, an improved *lux* operon for enhanced levels of bacterial bioluminescence

Carola Gregor[1], Klaus Gwosch[1], Stefan W. Hell[1]

[1] Department of NanoBiophotonics, Max Planck Institute for Biophysical Chemistry, Am Fassberg 11, 37077 Göttingen, Germany

Preface

The aim of this study was to improve the *lux* operon from *Photorhabdus luminescens* by mutagenesis in order to obtain higher levels of bacterial bioluminescence for single-cell imaging. The work was supervised by Prof. Dr. Stefan Hell. Dr. Klaus Gwosch built the microscope, programmed the software, aided with imaging, and performed the calibration. Mutagenesis, screening, cloning, sample preparation, and imaging were performed by me. I conceptualized and wrote this manuscript.

Chapter II: *ilux*, an improved *lux* operon for enhanced levels of bacterial bioluminescence

Carola Gregor[1], Klaus Gwosch[1], Stefan W. Hell[1]

[1] Department of NanoBiophotonics, Max Planck Institute for Biophysical Chemistry, Am Fassberg 11, 37077 Göttingen, Germany

Abstract

Besides the use of fluorescent proteins, bioluminescence microscopy is becoming an emerging tool for imaging of live cells. However, the luciferases which are mainly used currently require the addition of luciferins that are often toxic, expensive, poorly cell-permeable or produce high bioluminescence background signal. Bacterial bioluminescence is unique as it uses reduced FMN as a luciferin which is abundant in all cells, making this system purely genetically encodable. Unfortunately, the use of bacterial bioluminescence is limited by its low brightness compared to other luciferases. Here, we report the generation of an improved *lux* operon with a ~7-fold increase in brightness when expressed in *E. coli* cells at 37 °C. Besides addition of the *frp* gene from *Vibrio campbellii* to the *lux* operon from *Photorhabdus luminescens* that encodes an FMN reductase, *luxA, B, C*, and *frp* were improved by mutagenesis. The new version called *ilux* can be used to image single *E. coli* cells with enhanced spatiotemporal resolution for unlimited periods of time. In addition, since only living cells produce bioluminescent signal, we show that *ilux* can be used to observe the effect of different antibiotics on cell viability at single cell level in real time.

Introduction

Bioluminescence is a process in which cells generate light by a chemical reaction. It is catalyzed by an enzyme called luciferase and requires a luciferin substrate. The luciferin is converted into a product in an electronically excited state that emits a photon upon return to the ground state, thus emitting visible light. There are about 30 different luciferases and corresponding luciferins found in nature, indicating that bioluminescence has evolved several times independently during evolution [38], although in many cases its function remains

unknown. Most luciferins are only produced by organisms expressing the corresponding luciferase, with the exception of the bacterial luciferin $FMNH_2$. Bacterial luciferase is an αβ heterodimer that is coded by the genes *luxA* and *luxB*. In addition to $FMNH_2$, the reaction requires molecular oxygen and a long-chain fatty aldehyde. The fatty aldehyde is oxidized to a fatty acid and $FMNH_2$ is oxidized to FMN, thereby emitting a photon with a wavelength of λ_{max} ~490 nm:

$$FMNH_2 + RCHO + O_2 \rightarrow FMN + RCOOH + H_2O + hv$$

To keep this reaction ongoing, the fatty aldehyde must be regenerated. This is performed by the fatty acid reductase complex which consists of fatty acid reductase, transferase, and synthetase, coded by *luxC*, *luxD*, and *luxE*, respectively. Since an FMN reductase is already present in *E. coli*, introduction of the *luxCDABE* operon is sufficient to produce a bioluminescence output in these cells.

Due to its very low light levels compared to fluorescence, bioluminescence imaging is not routinely applied so far. Yet, bioluminescence provides several benefits compared to fluorescence measurements. First, there is virtually no background because of the lack of autofluorescence. Bioluminescence background levels in living cells are extremely low, making bioluminescence sometimes even more sensitive than fluorescence ([59] and references therein). Second, no excitation light source and filters are needed, making the setup very simple. In addition, it is possible to study processes where the intense excitation light required for fluorescence measurements would be disturbing, such as circadian rhythms or Ca^{2+} activity in the retina [63, 65]. Third, no phototoxicity or bleaching is observed, allowing image acquisition over arbitrary time spans. Furthermore, bioluminescence is dependent on cellular metabolism and hence only live cells are visible, preventing artifacts due to observation of severely damaged or dead cells.

In addition to the limitation by its low brightness, the luciferases that are most commonly used exhibit several drawbacks as the luciferin must be externally supplied. The luciferins are often expensive, toxic, poorly soluble, or cell-impermeable. Since the luciferin concentration is not stable over time, the signal often decays after only seconds or minutes. Therefore, the luciferin has to be applied repeatedly which complicates quantification of the signal. Moreover, coelenterazine, the substrate of *Renilla* and *Gaussia* luciferase, is auto-oxidized in solution, leading to background luminescence. Bacterial luciferase is the only luciferase that circumvents all these problems since FMN is present in all cell types and can be converted into $FMNH_2$ by the additional expression of an FMN reductase. Its main limitation is the poor

brightness which is several orders of magnitude lower than for other luciferases. Several attempts have been made to improve the brightness of bacterial bioluminescence, including splitting the *lux* operon for enhanced expression, codon-optimization for expression in mammalian cells, and exogenous addition of the fatty aldehyde [80-83]. However, to our knowledge, introduction of mutations in the *luxCDABE* operon to increase the brightness has so far been unsuccessful. Here, we demonstrate that bioluminescence from the *lux* operon from *Photorhabdus luminescens* expressed in *E. coli* can be substantially enhanced by co-expression of an FMN reductase and error-prone mutagenesis of the complete *lux* operon. The improved *lux* operon *ilux* can be used to image single *E. coli* cells for extended time periods and to assay cell viability in the presence of different antibiotics.

Results and Discussion

To engineer a bacterial bioluminescence system with improved brightness at 37 °C, we chose the *luxCDABE* operon from *P. luminescens* as this luciferase has been reported to be more thermostable than *Vibrio harveyi* luciferase [84]. The *P. luminescens luxCDABE* operon was cloned into the vector pGEX-6P-1. Expression in *E. coli* DH5α cells resulted in only weakly luminescent colonies. Since in this vector the fatty acid reductase coded by the *luxC* gene was expressed as a fusion protein with an N-terminal GST tag that may affect its function, we cloned the *luxCDABE* operon into an expression vector we named pGEX(-). This vector is based on pGEX-6P-1, but does not contain the GST tag. This increased the brightness ~40 % at room temperature and ~20-fold at 37 °C (Figure 20), suggesting that the activity of the fatty acid reductase is strongly inhibited by the large GST tag at elevated temperature, possibly by inhibiting assembly of the fatty acid reductase complex. In addition, we observed that the luminescence signal increases with temperature, yielding ~3 times more signal at 37 °C compared to room temperature. To further enhance the luminescence, we performed site-directed mutagenesis of multiple residues at the binding pocket in the luciferase α subunit and at the αβ interface. However, we were not able to identify mutants with increased luminescence signal (data not shown). Also random mutagenesis by error-prone PCR of the *luxAB* genes did not result in brighter variants, suggesting that the luciferase reaction might not be the rate-limiting step in the generation of bioluminescence light. To test this hypothesis, we cloned a second copy of *luxAB*, *CD*, *E* as well as an FMN reductase downstream of the *luxCDABE* operon and compared the brightness to the original construct. Both FMN reductase from *E. coli* and NADPH-flavin oxidoreductase from *Vibrio campbellii* coded by the *frp* gene

resulted in a ~1.5- and ~2.3-fold increase in brightness, respectively (Figure 20), showing that the endogenous FMN reductase in *E. coli* does not regenerate sufficient amounts of FMNH$_2$ for maximum levels of bioluminescence. We chose *luxCDABE+frp* pGEX(-) for mutagenesis and performed multiple rounds of error-prone PCR in the *luxAB*, *CD*, *E*, and *frp* genes. The resulting clones were screened for enhanced luminescence in DH5α cells on agar plates at 37 °C. We identified several mutations in *luxA*, *B*, *C*, and *frp* that resulted in higher bioluminescence signal, whereas no beneficial mutations in *luxD* and *E* were found. The final improved version called *ilux* contains the mutations listed in Table 3. Interestingly, the brightness of *ilux* was not only increased at 37 °C, but also at room temperature, showing that the introduced mutations not only enhance thermal stability of the enzymes, but mainly improve expression and folding or the catalytic activity.

These results indicate that not only the activity of the luciferase itself can be improved by mutagenesis, but also increasing the concentrations of FMNH$_2$ and fatty aldehyde by enhanced enzyme activities lead to higher bioluminescence. However, addition of myristate that is converted into tetradecanal by the fatty acid reductase complex in the cell did not further increase the brightness, either because the uptake is too slow or the concentration of tetradecanal does not limit the bioluminescence reaction any more. Also overexpression of the riboflavin transporter pnuX and addition of riboflavin to the medium to increase the cellular concentration of FMN showed no increase in brightness.

| gene	mutations
luxA	K22E, T119A, S178A
luxB	S13P, V121A, N259D
luxC	N10T, N59D, E74D, S256P, M355T, N360D
luxD	-
luxE	-
frp	M213L, R242L, K256R

Table 3: Mutations contained in *ilux*

The listed mutations were introduced by error-prone PCR into the *luxCDABE* operon from *P. luminescens* supplemented with the *frp* gene from *V. campbellii*, resulting in the improved operon *ilux*.
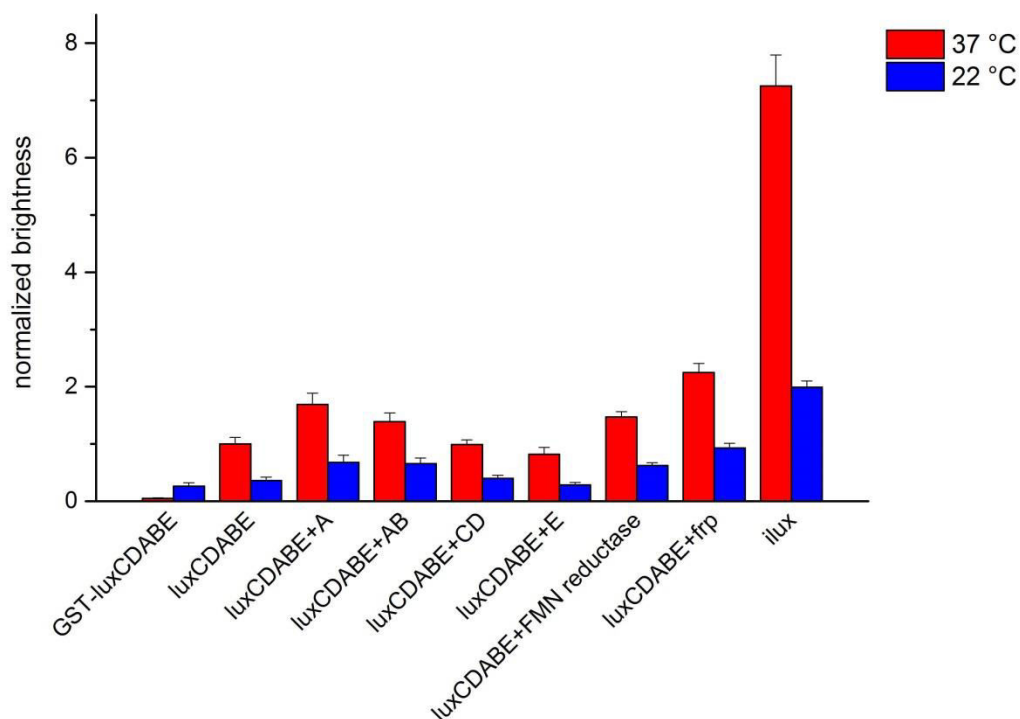
Figure 20: Brightness of different *lux* variants expressed from pGEX(-) in DH5α cells

luxCDABE with a second copy of the indicated genes were expressed from pGEX(-) in DH5α cells. 6 colonies of each construct were spread on a new agar plate. After growth over night at 37 °C, plates were imaged at 37 °C and 22 °C. The signal from 3 different areas for each clone was averaged. Error bars represent standard deviation.

After several rounds of screening, we did not obtain further improvements by error-prone mutagenesis in any of the *luxCDABE+frp* genes. A possible explanation is that at least one of the *lux* proteins is already optimized under the screening conditions and limits the overall reaction, or the number of possible additional beneficial mutations is so low that we were not able to identify them in our screening. To obtain higher levels of expression for imaging of single *E. coli* cells, the *ilux* operon was cloned into the vector pQE(-). This vector was generated from pQE30 by deletion of the His tag. Expression of *ilux* from pQE(-) in *E. coli* Top10 cells resulted in a ~2.3-fold higher signal at room temperature compared to pGEX(-) in DH5α on agar plates. Although the bioluminescence intensity is higher at 37 °C, imaging was performed at room temperature for technical reasons. Single Top10 cells can already be discriminated after only 10-20 s (Figure 21). Longer exposure times result in significantly improved signal-to-noise ratio. A calibration of the camera indicates that 100–200 photons per pixel are detected during a 10 min exposure time, corresponding to ~4·10^3 detected photons per cell per minute.
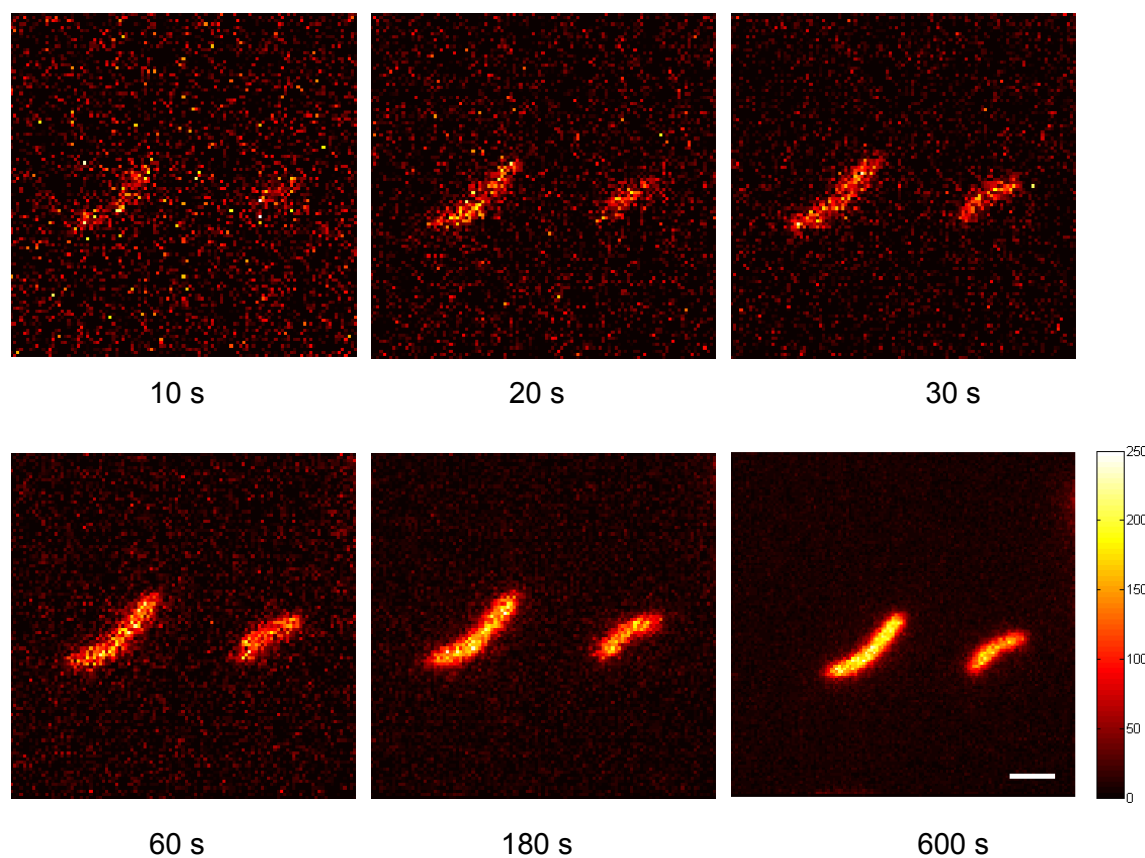
Figure 21: *E. coli* Top10 cells with *ilux* pQE(-) imaged for different exposure times.

E. coli Top10 cells with *ilux* pQE(-) were imaged under an LB agar pad containing 50 µg/ml ampicillin. Single images were taken with the indicated exposure times. For the 10 min image, the colorbar represents the approximate number of detected photons. For the other images, the contrast was adjusted manually. Scale bar, 2 µm

We used exposure times of 10 min to observe cells over longer time spans. Most cells remained viable over the whole recording time of 12 h and divided several times (Figure 22).

0 h   2.5 h   4.8 h

7.2 h   9.5 h   12 h
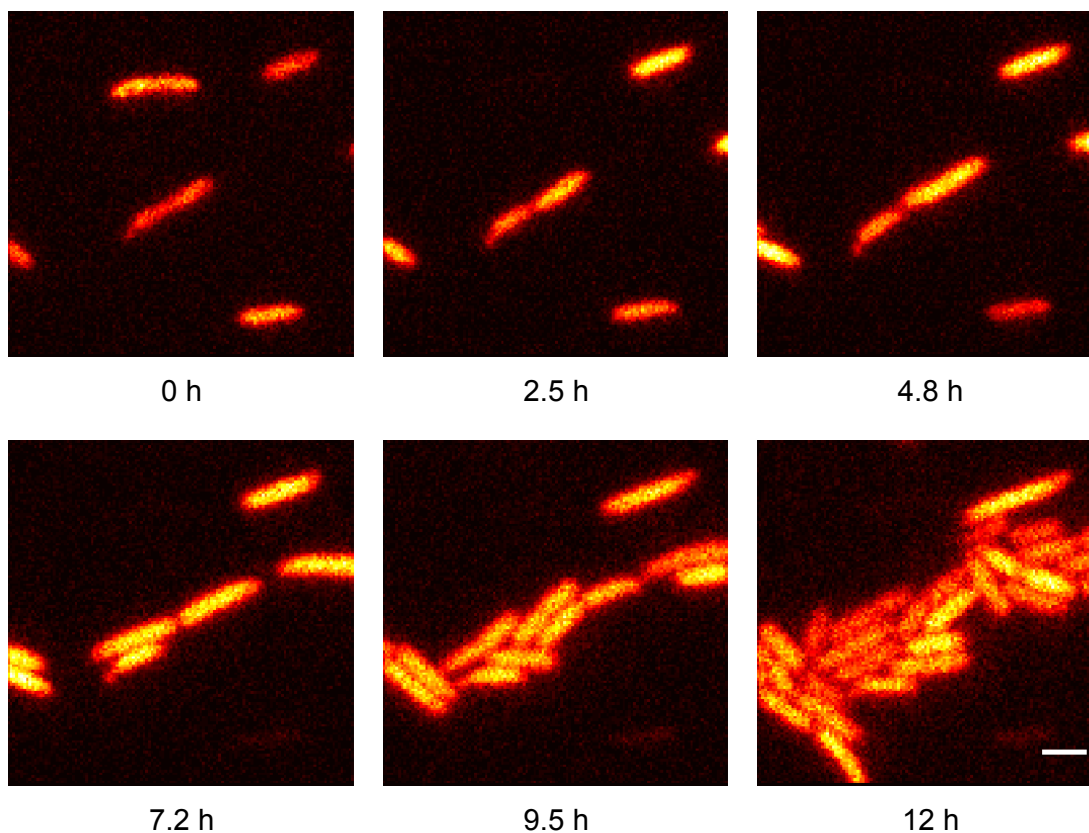
Figure 22: Cell division of *E. coli* cells expressing *ilux*

E. coli Top10 cells with *ilux* pQE(-) were imaged under an LB agar pad containing 50 µg/ml ampicillin. Single images were taken with 10 min exposure time. The same colormap was used for all images. Scale bar, 2 µm

Subsequently, we investigated the effect of different antibiotics on cell viability. Since continuous supply of ATP and NADPH is required for regeneration of fatty aldehyde and $FMNH_2$ to keep the bioluminescence reaction ongoing, the signal is expected to disappear upon cell death. First, we imaged Top10 cells in the presence of 100 µg/ml kanamycin which inhibits protein synthesis (Figure 23). The brightness decreased continuously, indicating a reduction in metabolic activity. Most cells died within the 45 h observation time, nevertheless, bioluminescence was still detectable from a few cells. This demonstrates that even at high kanamycin concentrations cellular metabolism continues for relatively long time spans, although cell division is prevented immediately.

0 h   6 h   12 h

18 h   24 h   45 h
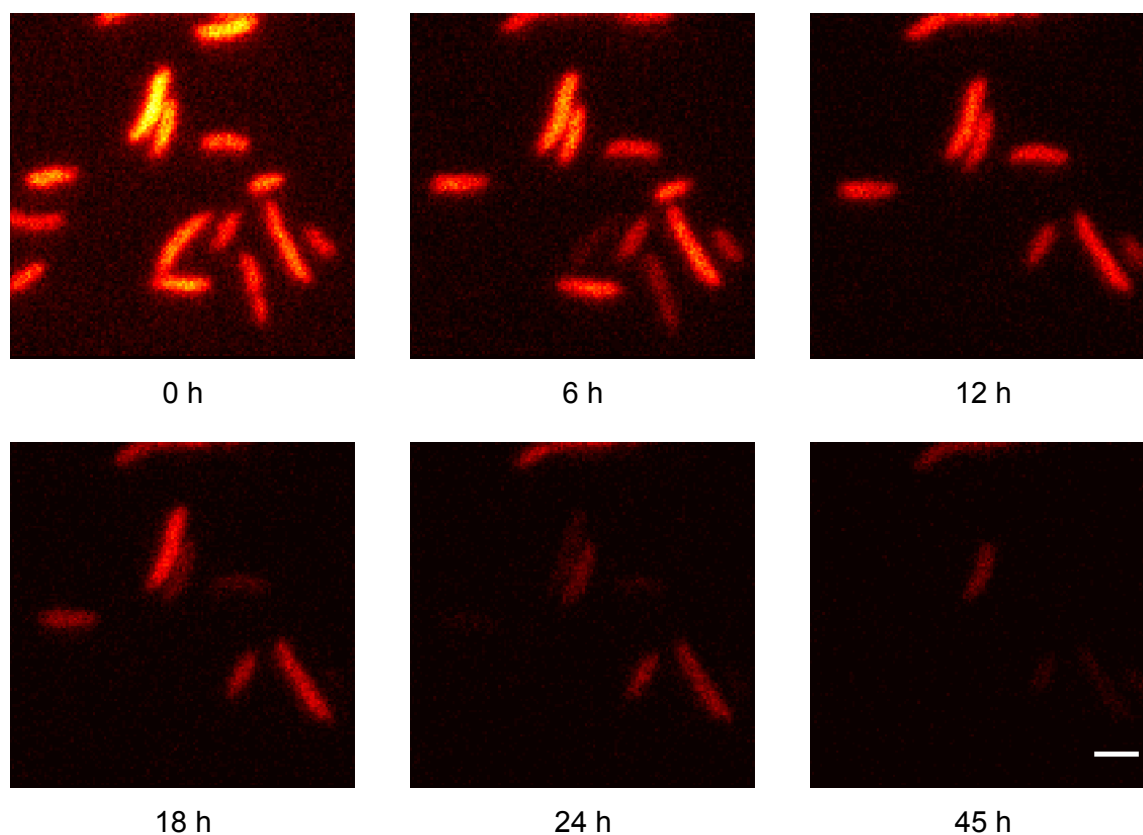
Figure 23. *E. coli* cells expressing *ilux* in the presence of kanamycin

E. coli Top10 cells with *ilux* pQE(-) were imaged under an LB agar pad containing 50 µg/ml ampicillin and 100 µg/ml kanamycin. Single images were taken with 10 min exposure time. The same colormap was used for all images. Scale bar, 2 µm

The second antibiotic we examined is timentin, a mixture of the β-lactame antibiotic ticarcillin and clavulanic acid. Since pQE(-) contains β-lactamase as a resistance marker, cells expressing *ilux* are expected to be resistant to ticarcillin. However, since the β-lactamase is inhibited by clavulanic acid, the cells become susceptible for the cell wall-disrupting effects of ticarcillin and ampicillin. Upon cell division, this leads to formation of small holes in the cell wall. As a result, the inner membrane occasionally forms large protrusions due to osmotic pressure (Figure 24). This finally leads to cell lysis. After 12 h, all cells had died.

| 0 h | 2.3 h | 4.7 h |
| 7.0 h | 9.3 h | 11.7 h |

Figure 24. *E. coli* cells expressing *ilux* in the presence of 100 µg/ml timentin

E. coli Top10 cells with *ilux* pQE(-) were imaged under an LB agar pad containing 50 µg/ml ampicillin and 100 µg/ml timentin. Single images were taken with 10 min exposure time. The same colormap was used for all images. Scale bar, 2 µm
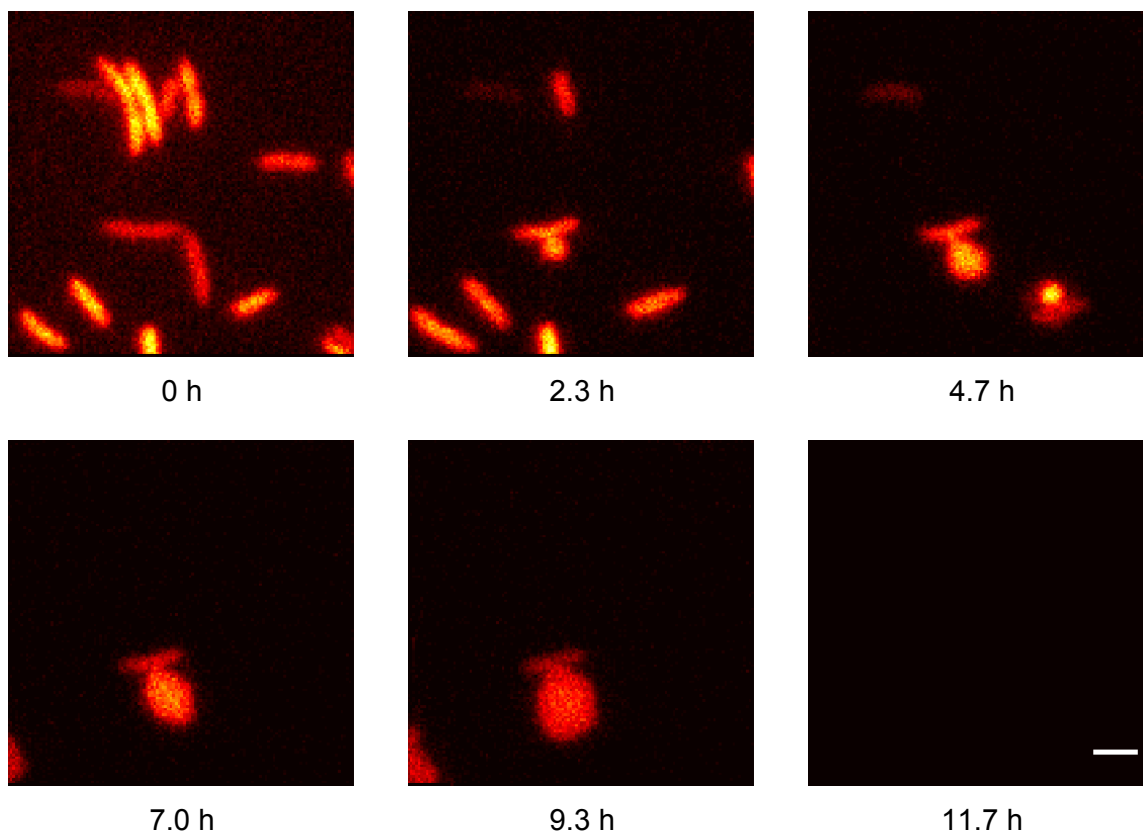
Interestingly, we often observed "blinking" of the cells before cell death. The signal from from cells that had already disappeared completely often recovered, sometimes even between two 10 min frames (Figure 25). Since ATP and NADPH are required for bioluminescence, this possibly indicates that *E. coli* cells can temporarily recover after breakdown of their energy metabolism, although complete cell death usually occurred within few hours thereafter.

Figure 25: "Blinking" of *E. coli* cells during kanamycin-induced cell death

E. coli Top10 cells with *ilux* pQE(-) were imaged under an LB agar pad containing 50 µg/ml ampicillin and 100 µg/ml kanamycin. Single images were taken with 10 min exposure time. The same colormap was used for all images. Scale bar, 2 µm
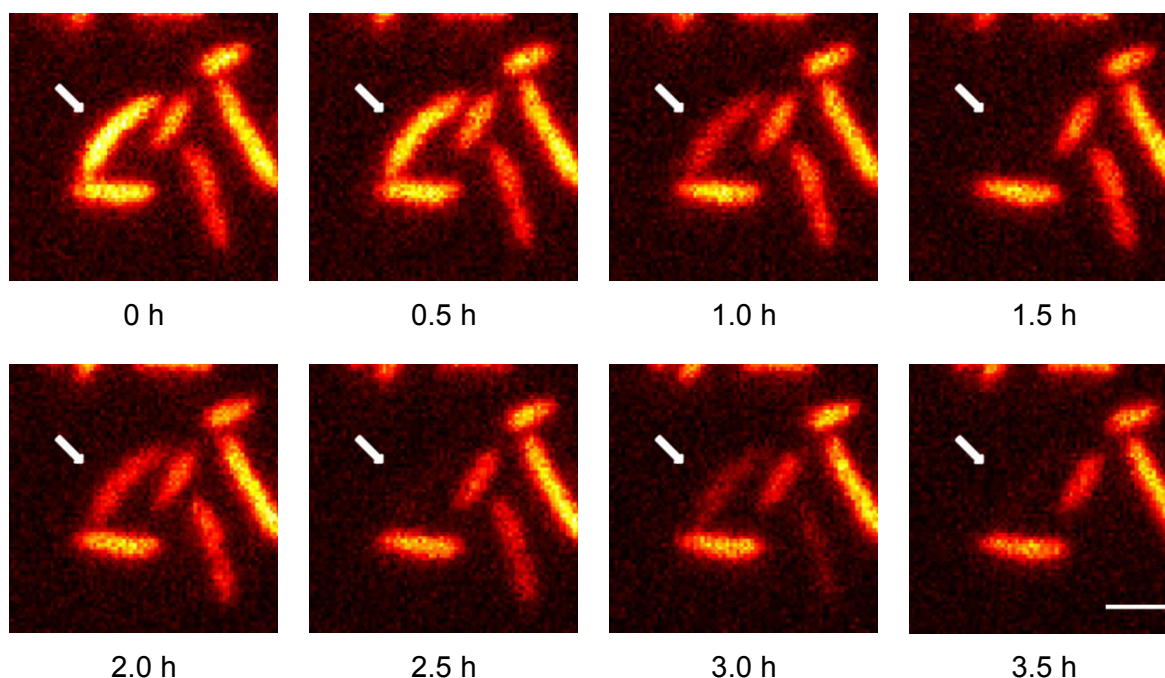
Our results show that bacterial bioluminescence can be enhanced by mutagenesis of the *luxCDABE* genes in combination with introduction of an additional FMN reductase into *E. coli*. This allows imaging of single *E. coli* cells with improved spatiotemporal resolution in comparison to previous approaches of single-cell imaging [65, 83]. Since the brightness of *ilux* is increased ~3-fold at 37 °C compared to room temperature, heating of the sample during imaging is expected to reduce the necessary recording times even further. We have demonstrated that *ilux* can be used to study processes such as cell division and cell death, extending the range of applications of bioluminescence imaging. The independence of exogenous luciferin makes the *lux* system particularly interesting, although its utility has been limited by its low brightness compared to other luciferases. Codon-optimized versions of the *lux* proteins have been shown to be functional in eukaryotic cells [81, 82], facilitating observation of bacterial bioluminescence from cell types other than bacteria. Therefore, *ilux* is promising to be a valuable tool for the observation of mammalian cells as well. In addition, it might be possible to image cellular structures by fusing the luciferase α subunit or a fusion of α and β subunit to a protein of interest, allowing its usage in a similar way as GFP.

Materials and Methods

Cloning and Mutagenesis

The vector pGEX(-) was generated by PCR of pGEX-6P-1 with the primers pGEX(-) BamHI fwd / pGEX(-) BamHI rev (Table 4). The PCR product was digested with DpnI to remove template DNA and gel-purified. The obtained DNA fragment was digested with BamHI and ligated without an insert to obtain pGEX(-). pQE(-) was generated from pQE30 in an analogous way using the primers pQE(-) BamHI fwd / pQE(-) BamHI rev.

luxCDABE was amplified with the primers luxC BamHI fwd / luxE SalI rev and cloned into pGEX-6P-1 and pGEX- with BamHI and SalI. The *frp* gene was introduced behind *luxE* between the SalI and NotI restriction sites with the primers frp SalI fwd and frp NotI rev. Second copies of *luxA*, *AB*, *CD*, and *E* were also cloned between the SalI and NotI restriction sites using the primers luxA SalI fwd / luxA NotI rev, luxA SalI fwd / luxB NotI rev, luxB SalI fwd / luxB NotI rev, luxC SalI fwd / luxD NotI rev, and luxE SalI fwd / luxE NotI rev, respectively.

For error-prone PCRs, an EcoRI restriction site was introduced in front of *luxA* by PCR of the whole plasmid with the primers luxA EcoRI fwd and linker luxDA EcoRI rev, digesting the PCR product with DpnI and EcoRI and ligation without an insert. Similarly, an NcoI restriction site behind *luxB* were introduced with the primers linker luxBE NcoI fwd and luxB NcoI rev.

Error-prone PCRs were performed with the following primers:

luxAB: EP luxAB EcoRI fwd / EP luxAB NcoI rev

luxCD: EP luxCD BamHI fwd / EP luxCD EcoRI rev

luxE: EP luxE NcoI fwd / EP luxE SalI rev

frp: EP frp SalI fwd / EP frp NotI rev

25 PCR cycles were performed with $MnCl_2$ concentrations ranging from 50 µM to 150 µM. The PCR products were gel-purified, digested with the indicated enzymes, and ligated back into the *lux* pGEX(-) vector.

An XmaI restriction site behind the *frp* gene was introduced by PCR of *frp* with the primers frp SalI fwd / frp XmaI NotI rev and cloning the PCR product back into the vector with SalI and NotI. pnuX was cut from a template vector with AgeI and NotI and integrated between the XmaI and NotI restriction sites. The complete *ilux* operon was cut with BamHI and XmaI and ligated into pQE(-) digested with the same enzymes.

pGEX(-) BamHI fwd	CAGGGGCCCCTGGGATCCCCGGAATTCCCG
pGEX(-) BamHI rev	TATAGGGGACATGGATCCTGTTTCCTGTGT
pQE(-) BamHI fwd	CGTAATGGATCCGCATGCGAGCTCG
pQE(-) BamHI rev	GTTCAGGGATCCAGTTAATTTCTCCTCTTTAATGAATTCTGTGT
luxC BamHI fwd	TTAGATGGATCCATGACTAAAAAAATTTCA
luxE SalI rev	TCTTAGGTCGACTCAACTATCAAACGCTTC
frp SalI fwd	GTAACTGTCGACCTAAGGAGAAAGAAATGGTGAAGATACAG
frp NotI rev	CTTAGAGCGGCCGCTTACCTTTTGGCAAGGC
luxA EcoRI fwd	TGTATCGAATTCATGAAATTTGGAAACTTTTTG
linker luxDA EcoRI rev	TGTATCGAATTCAGAGAGTCCTTATATTGCTAT
linker luxBE NcoI fwd	TGTATCCCATGGTAGATTTCGAGTTGCAGCGAG
luxA SalI fwd	GTAACTGTCGACCTAAGGAGAAAGAAATGAAATTTGGAAACTTTTTGC
luxA NotI rev	GTAAGTGCGGCCGCCTAATATAATAGCGAACGTTGTT
luxB NotI rev	CTTAGAGCGGCCGCTTAGGTATATTCCATGTGGTAC
luxC SalI fwd	GTAACTGTCGACCTAAGGAGAAAGAAATGACTAAAAAAATTTCATTCATTATTAACG
luxD NotI rev	CTTAGAGCGGCCGCTTAAGACAGAGAAATTGCTTG
luxE SalI fwd	GTAACTGTCGACCTAAGGAGAAAGAAATGACTTCATATGTTG
luxE NotI rev	CTTAGAGCGGCCGCTCAACTATCAAACGCTTC
luxB NcoI rev	TGTATCCCATGGTTAGGTATATTCCATGTGGTA
EP luxAB EcoRI fwd	GCAATATAAGGACTCTCTGAATTC
EP luxAB NcoI rev	GCTGCAACTCGAAATCTACCATGG
EP luxCD BamHI fwd	GGGCCCCTGGGATCC
EP luxCD EcoRI rev	TTTCATGAATTCAGAGAGTCCTTATATTGCTATTTGAGTG
EP luxE NcoI fwd	ACCTAACCATGGTAGATTTCGAGTTGCAGC
EP luxE SalI rev	GCGGCCGCTCGAGTCGAC
EP frp SalI fwd	GTAACTGTCGACCTAAGGAGAAAGAAATGGTGAAGATACAG
EP frp NotI rev	CTTAGAGCGGCCGCTTACCTTTTGGCAAGGC
frp XmaI NotI rev	CTTCATGCGGCCGCTATCCACCCGGGTTCTTTCTCCTTAGTTACCTTCTGGCAAGGCCC

Table 4: Primers used for cloning and error-prone PCRs

Imaging

Screening for brighter variants was performed with *E. coli* DH5α cells expressing *lux* proteins from pGEX(-). Colonies on agar plates were grown and imaged at 37 °C with a PCO Sensicam (LaVision). The brightest clones were selected for the next cycle of mutagenesis.

For single-cell imaging, *E. coli* Top10 cells containing *ilux* pQE(-) were grown over night at 37 °C on LB agar plates containing 50 µg/ml ampicillin and 100 µg/ml carbenicillin to prevent loss of the plasmid. Cells from the agar plate were resuspended in water. 1 µl of the suspension was placed on a coverslip, covered with an agar pad cut from an LB agar plate, and immediately used for imaging.

Imaging was performed with a self-built setup (see Figure 26). An EMCCD camera (iXon DU860, Andor) was used for detection that was cooled to -93 °C. Readout was performed in kinetics mode using a vertical shift speed of 0.1 µs/pixel and a horizontal readout speed of 1 MHz. The pre-amp gain was set to 5 and the EM gain was set to 300 (Real EM gain mode). The effective pixel size of the camera was 120 nm.

A 405 nm excitation laser (PhoxX 405-60, Omicron) was used to select and focus the cells. The laser was focused to the back focal plane of the objective resulting in an illumination area in the sample of about 20 µm in diameter. The utilized laser power in the back focal plane of the objective was 290 nW. To keep the sample in the same z-position during long-term imaging, a home-built focus lock was used. The focus lock system measured the axial position of the sample by measuring the position of a total internal reflection (TIR) signal at the coverslip-media interface. For this purpose, a 980 nm laser beam was focused off-center into the back focal plane of the objective lens. The TIR signal was detected by a position sensitive diode. A feedback loop written in Python calculated the necessary shift of the objective to compensate for drifts of the focal plane. The axial position of the objective lens was updated every 100 ms commanding the objective positioner piezo (MIPOS 100 PL CAP, piezosystem Jena).

Light from the sample was collected with a HC PL APO 100x/1.40-0.70 OIL CS oil immersion objective lens (Leica). The light was directed to the camera using dielectric mirrors (BB1-E02, Thorlabs), a dichroitic beam splitter (ZT405rdc, Chroma), and a detection filter (BrightLine FF01-842/SP, Semrock) to block light from the focus lock laser. The first mirror after the objective lens was a back side polished version (BB1-E02P, Thorlabs) to allow in- and outcoupling of the 980 nm focus lock. Focusing onto the camera was performed with an achromatic lens with a focal length of f = 400 mm and VIS coating (Qioptiq) resulting in an effective pixel size on the camera of 120 nm. Measurement control and data acquisition were performed with self-written Python programs.

To filter out bright pixels due to cosmic radiation, the value of pixels above a brightness threshold was replaced by the average of the same pixel in the previous and following image. Unless otherwise stated, the average background signal from the same exposure time without sample was subtracted.

Calibration of camera pixel values to detected photons was performed by measuring the mean and variance of the pixel values of a uniformly illuminated camera sensor chip for several exposure times.

Assuming Shot noise for conditions when background counts are negligible, variance and mean of the pixel values N_{ADC} are proportional to each other:

$$\text{var}(N_{ADC}) \propto 2 \cdot \alpha \cdot \text{mean}(N_{ADC})$$

The proportionality factor α given by the ADC counts per photoelectron and can be obtained by a linear fit to the data. The factor 2 accounts for the excess noise factor of 1.41 of an EMCCD camera. The mean of the camera count offset μ_{offset} was obtained from camera images without illumination. Finally, the conversion of camera ADC counts N_{ADC} to photons N_{photon} was performed by

$$N_{photon} = \alpha^{-1}\left(N_{ADC} - \mu_{offset}\right)$$

with the definitions given above.
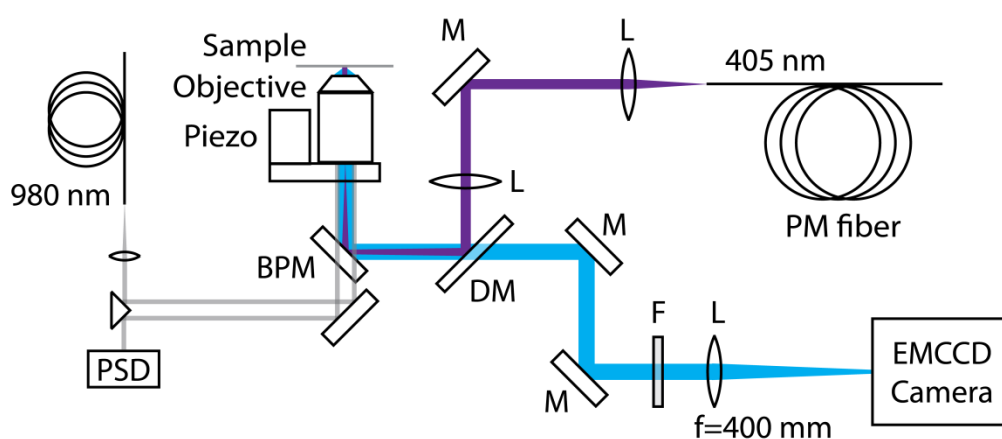
Figure 26: Schematic setup of the microscope

Bioluminescence light is collected by an oil immersion objective lens and directed to an EMCCD camera using dielectric mirrors (BPM, M) optimized for the visible wavelength range. The light is spectrally filtered by a shortpass filter (F) and focused onto the camera using a lens (L) with a focal length of 400 mm. For focusing and selection of cells, a widefield excitation with 405 nm is implemented. A dielectric mirror (DM) is used to separate excitation light from fluorescence. Long term stability of the focus position is provided by a home-built focus lock system. It is based on the detection of a total internal reflection signal using a position sensitive diode (PSD) and repositioning the objective lens with a z-piezo. In- and outcoupling of the 980 nm light for the focus lock is done through a back side polished dielectric mirror (BPM).

Discussion

In the previous chapters, the utility of flavin-binding proteins for different kinds of microscopy has been demonstrated. Considerable improvements in brightness were achieved by mutagenesis, opening new fields of application of flavin-based proteins in superresolution and bioluminescence microscopy.

RESOLFT microscopy with RSFPs has so far been only performed with proteins from the GFP superfamily [71-74]. GFP-based proteins exhibit high brightness and many different variants have been developed that cover the whole visible spectral range [85], making them excellent tools for the imaging of living cells. However, GFP-related proteins share several features that restrict their applicability under certain conditions. These include their relatively large size (27 kDa), dependence on oxygen for chromophore maturation, and quenching of their fluorescence at low pH. Therefore, the development of new fluorescent proteins with different properties from other origin is desirable for certain applications.

A new class of fluorescence reporters are FbFPs which are derived from LOV domains and contain a flavin chromophore. They are small (10–19 kDa) and oxygen-independent and their fluorescence is relatively constant over a broad pH range, but they exhibit generally lower brightness than GFP-based proteins [1, 35]. Due to their inherent photoswitching, LOV domains are also interesting for superresolution microscopy. This was demonstrated for the first time with the LOV domain of the photoreceptor YtvA from *B. subtilis* where the wild-type protein was used for PALM imaging [36]. YtvA-LOV can in principle also be used for RESOLFT microscopy, but its use is impeded by its relatively low brightness combined with an on-switching of only ~5 %. In chapter I of this thesis, it was shown that the on-switching of YtvA-LOV could be improved by mutagenesis, resulting in the new RSFP rsLOV1 (Figure 27). rsLOV1 switches off with little switching background (< 3 %) and switches both on and off ~3 times faster than rsEGFP2, the fastest switching RSFP published so far, making it interesting for fast RESOLFT imaging. The fraction of on-switching under 405 nm illumination was increased by a factor of ~10 for rsLOV1 compared to YtvA-LOV wt, resulting in a ~10-fold increase in brightness under RESOLFT imaging conditions. Its applicability for RESOLFT imaging with a resolution of down to ~60–65 nm was proved in chapter I.

Despite these improvements, the brightness of rsLOV1 is still relatively low. Its brightness is only ~6 % of EGFP in the fluorescent on-state (ε_{rsLOV1} = 11,000 $M^{-1} \cdot cm^{-1}$, ϕ_{rsLOV1} = 0.17, ε_{EGFP} = 55,000 $M^{-1} \cdot cm^{-1}$, ϕ_{EGFP} = 0.60 [77, 78]). The effective brightness under RESOLFT

imaging conditions was even further reduced by incomplete on-switching (~57 % of the initial signal) and excitation at 488 nm instead of the absorption maximum of 450 nm. Therefore, the sample had to be scanned multiple times during image acquisition to accumulate sufficient signal, nullifying the advantage of ultrafast switching of rsLOV1 for fast imaging.
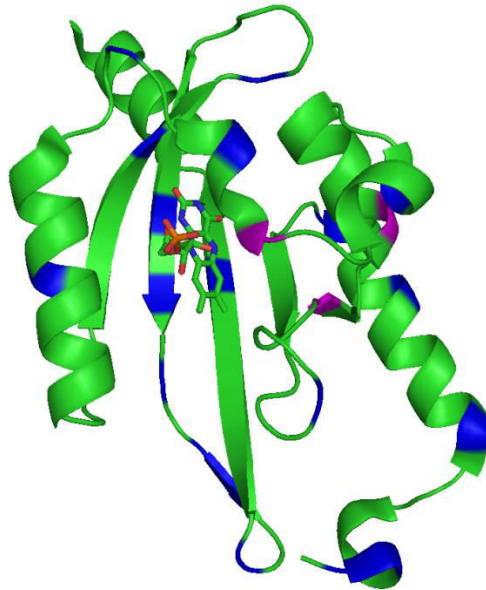
Figure 27: Mutations of rsLOV1 and rsLOV2 based on the structure of YtvA-LOV (aa 1–137)
The first 137 residues of YtvA-LOV wt (PDB entry 2MWG [28]) containing the FMN cofactor are shown. Positions of the mutations in rsLOV1 are shown in blue. Additional mutations in rsLOV2 are marked in purple.

Further improvements in brightness are therefore favorable that might be achieved by continued mutagenesis. However, mutagenesis has been done extensively in this work, including multiple rounds of error-prone mutagenesis, site-directed saturation mutagenesis of all single residues, exchange of the N- and C-terminal regions, and exchange of a loop region (aa 32–37), without further improvements in brightness. A different approach for increasing the brightness is exchange of the cofactor. Modified flavin cofactors with higher quantum yields than FMN have been synthesized and incorporated into YtvA-LOV *in vitro* [12, 79]. Yet, modified flavins would need to be taken up and incorporated into the protein under cellular conditions. This might be inefficient and result in only a small fraction of the protein containing the modified cofactor. Moreover, some flavin derivatives such as roseoflavin are toxic and therefore undesirable for live-cell imaging. In addition, the photocycle can be influenced by exchange of the cofactor [12] so that additional mutagenesis and screening may be required for optimal switching. Another possible way to obtain brighter LOV-based proteins is the

choice of a different template for mutagenesis. FbFPs have been generated from LOV domains of different origin [30-33] with quantum yields of up to 51 % [33]. However, their increased brightness is partially due to removal of the photoactive cysteine residue required for switching. Therefore, it remains questionable by how much the brightness of flavin-binding RSFPs can be further improved.

Another variant of YtvA-LOV was described in chapter I of this work. This protein, named rsLOV2, contains three additional mutations compared to rsLOV1 (I39V, Q44N and N61S), indicated in Figure 27. rsLOV2 is approximately twice as bright as rsLOV1 in its fluorescent on-state (ε_{rsLOV2} = 11,000 $M^{-1} \cdot cm^{-1}$, ϕ_{rsLOV2} = 0.31) and switches on even more efficiently than rsLOV1. Unfortunately, its switching background is relatively high and strongly increases after repeated switching or prolonged illumination with UV light, making it unsuitable for RESOLFT imaging. It was shown that rsLOV2 can be used for STED imaging of living cells instead, achieving a resolution of down to 40–50 nm. Interestingly, imaging could be performed with 488 nm excitation and 618 nm STED only, omitting the on-switching at 405 nm. This indicates that a fraction of rsLOV2 accumulates in a fluorescent state under imaging conditions, although the reasons for this remain unknown and may include nonlinear processes due to the high STED intensity. The complex photocycle of YtvA-LOV was studied in detail [25], but is still not fully understood. Furthermore, the photochemistry of rsLOV2 is different than for the wild-type protein, making it difficult to predict transitions into certain states.

Since protein screening was performed with the aim to optimize switching and brightness for RESOLFT microscopy, it is likely that rsLOV2 and other LOV domains can be further optimized for STED applications. Due to the unpredictable behavior under different conditions, screening for brighter and more photostable LOV variants should be performed under the same conditions as used for STED imaging. The high photostability of rsLOV2 under the applied imaging conditions makes FbFPs promising for the development of valuable alternatives to GFP-based fluorescent proteins for STED microscopy.

In the second part of this work, the usefulness of bacterial bioluminescence for microscopy was demonstrated. Although bioluminescence has been studied for decades, it has received relatively little attention for the purpose of imaging so far. This is mainly due to its relatively low light levels compared to fluorescence and because exogenous luciferins must often be added. Fluorescent proteins have been used extensively to image living cells since they are non-toxic, relatively small, genetically encodable, can be expressed as fusion proteins with a specific protein of interest, and produce strong fluorescence when excited with intense light.

Discussion

However, fluorescence measurements are not optimal for all purposes. For some applications, the excitation light would disturb the process that is to be observed and for long-term measurements bleaching can be a problem. Bioluminescence imaging complements the potential applications of fluorescent proteins and can also be combined with them for imaging. Due to the limitation by their low brightness, several attempts were made to improve naturally occurring luciferases by mutagenesis. For firefly luciferase which has the highest bioluminescence quantum yield known (~0.40 [86]), this has so far been unsuccessful and it was suggested that this enzyme may be nearly optimized by natural evolution [59]. An improved luciferase called NanoLuc, however, has been generated from a fragment of the luciferase from the deep sea shrimp *Oplophorus gracilirostris*. This was achieved by mutagenesis as well as chemical modification of its natural luciferin coelenterazine [87]. NanoLuc has also been used for dual color bioluminescence imaging in combination with firefly luciferase [88]. Other approaches to increase bioluminescence intensity have mainly focused on enhancing the expression in other cell types by codon-optimization [81, 89, 90]. Bacterial bioluminescence, which is particularly interesting because it does not require the addition of an exogenous luciferin, has so far been improved by addition of an FMN reductase to a codon-optimized version of the *luxCDABE* operon for expression in mammalian cells [81, 82], splitting the *luxCDABE* operon for generating higher concentrations of the rate-limiting aldehyde [80], and exogenous addition of tetradecanal or other long-chain fatty aldehydes [80, 83]. However, to my knowledge, no approaches to enhance the activity of the involved proteins by mutagenesis have been reported.

In this work, it was shown that bacterial bioluminescence originating from the *luxCDABE* operon from *P. luminescens* expressed in *E. coli* could be improved by mutagenesis. This was achieved by integration of an FMN reductase into the *lux* operon and subsequent error-prone mutagenesis of the *luxA*, *B*, *C*, and *frp* genes. It was demonstrated that the brightness could be substantially improved, resulting in a ~7-fold yield of bioluminescence at 37 °C. This was used to study the effects of different antibiotics on cell viability since only cells with an intact metabolism emit bioluminescence light. Viability of bacteria is usually assayed by their ability to divide because methods to monitor their metabolic state on the single-cell level are lacking. Yet, non-dividing cells may still be metabolically active and a 'viable but non-culturable' (VBNC) state has been hypothesized from which non-dividing cells may be 'resuscitated', although the existance of this state is controversial [91]. An approach to observe ATP levels in single bacteria using a Förster resonance energy transfer (FRET)-based ATP biosensor has been described [92]. In this study, it was found that after antibiotic treatment not all non-

growing bacteria with low ATP levels stained with propidium iodide (PI), a widely used fluorescent live/dead cell marker. Since PI is membrane impermeable, only dead cells with damaged membranes are stained. In addition, it was found that a subset of PI-negative cells with high ATP levels did not resume growth after antibiotic washout [92]. This indicates that PI is not an optimal marker for assaying bacterial viability. It is known that subpopulations of bacteria (called persisters) escape killing by antibiotics although they are not genetically resistant [92]. As antibiotic resistances are an increasing problem for public health, the development of new antibiotics and methods to test their impact on single bacterial cells are required. Using the *ilux* proteins developed in this work, it was observed that *E. coli* cells can temporarily recover from metabolic inactivity sometimes occuring before cell death. Although it cannot be ruled out completely that other effects account for this observation, *ilux* is a useful alternative to fluorescent reporters for long-term investigations of single bacteria.

It is not yet clear if the brightness of bacterial bioluminescence can be further enhanced. To test if one of the *lux* proteins is already optimized and limits the overall reaction, second copies of the improved *luxA*, *B*, *C*, *D*, *E, AB*, *CD*, and *frp* genes were cloned into *ilux* pGEX(-). However, none of these constructs showed a significant increase in brightness (data not shown). This may be due to inefficient expression of the second copies due to their large distance from the promotor or the cells may regulate cellular levels of the *lux* enzymes and degrade proteins at higher concentrations. A different explanation is that the brightness is not limited by the *ilux* proteins themselves, but by another process. Since NADPH is required for regeneration of fatty aldehyde and $FMNH_2$, an attempt to increase cellular levels of NADPH by overexpressing glucose-6-phosphate dehydrogenase, the key enzyme of the pentose phosphate pathway, was made. Yet, no increase in brightness was observed (data not shown), probably because the level of this metabolic protein is tightly regulated. Possibly the supply of cells with nutrients when grown in colonies on agar plates is limiting for the bioluminescence reaction due to slow diffusion from the agar into the cells. However, this is in contradiction to the observation that colonies of Top10 cells expressing *ilux* from pQE(-) are ~3-fold brighter than *ilux* pGEX(-) in DH5α cells, a fact that may be attributed to higher expression. Perhaps there are also differences between the *E. coli* strains allowing for higher bioluminescence yields in Top10 cells. Alternatively, the pGEX(-) plasmid may get lost more easily during cell division, resulting in lower signal in DH5α cells because not all cells express the *ilux* proteins. Further experiments are therefore required to identify the rate-limiting step and to potentially further increase the brightness of bacterial bioluminescence.

Discussion

Although bacterial luciferase has the disadvantage to be dimeric, it may be used to label structures within living cells. This could either be achieved by fusion of the α subunit or a fusion protein of α and β subunit to the protein of interest. Monomeric bacterial luciferases consisting of fused α and β subunit separated by different linkers were reported to be active, although sometimes having significantly reduced activity, depending on the type of bacterial luciferase, length and sequence of the linker, and temperature [84, 93]. In addition, the improved *ilux* proteins should also be applicable in mammalian cells after codon-optimization and therefore extend their use beyond imaging of bacterial cells.

Other ways to modify bacterial bioluminescence are the generation of red-shifted mutants that would be superior for imaging of living animals due to better penetration of tissue for red light. However, the potential spectral shifts are likely to be of minor influence due to the small size and rigidity of the flavin chromophore. The introduction of artificial flavins with different spectral properties as discussed for LOV domains may be possible, but at the expense of making the *lux* system dependent on an exogenous luciferin. Another way to red-shift the emission and at the same time possibly enhance the overall quantum yield is the co-expression of a fluorescent protein like YFP (yellow fluorescent protein) as an acceptor and light emitter after resonance energy transfer.

A different way for generating autonomous bioluminescence from enzymes other than bacterial luciferase is the synthesis of other luciferins in the cell. Since all luciferins are synthesized by cells in nature, co-expression of all enzymes that are involved in their biosynthesis would circumvent the requirement of luciferin addition. In this way, bioluminescence from other luciferases could be made completely genetically encodable and therefore expand their use for live cell imaging.

References

1. Mukherjee, A., et al., *Characterization of flavin-based fluorescent proteins: an emerging class of fluorescent reporters.* PLoS One, 2013. **8**(5): p. e64753.

2. *Flavins and flavoproteins: methods and protocols,* ed. S. Weber and E. Schleicher. 2014, New York: Springer.

3. Said, H.M., et al., *Riboflavin uptake by human-derived colonic epithelial NCM460 cells.* Am J Physiol Cell Physiol, 2000. **278**(2): p. C270-6.

4. Voet, D. and J.G. Voet, *Biochemistry*. 3 ed. 2004: John Wiley & Sons.

5. van Pee, K.H. and E.P. Patallo, *Flavin-dependent halogenases involved in secondary metabolism in bacteria.* Appl Microbiol Biotechnol, 2006. **70**(6): p. 631-41.

6. Mansoorabadi, S.O., C.J. Thibodeaux, and H. Liu, *The diverse roles of flavin coenzymes - nature's most versatile thespians.* J. Org. Chem., 2007. **72**(17): p. 6329 - 6342.

7. Sancar, A., *Structure and function of DNA photolyases and cryptochrome blue-light photoreceptors.* Chem Rev., 2003. **103**(6): p. 2203-37.

8. Fagan, R.L. and B.A. Palfey, *Flavin-dependent enzymes*. Comprehensive natural Products II, ed. T.P. Begley. Vol. 7. 2010, New York: Elsevier Ltd.

9. Massey, V., *The chemical and biological versatility of riboflavin.* Biochem Soc Trans, 2000. **28**: p. 283-96.

10. Losi, A. and W. Gärtner, *The evolution of flavin-binding photoreceptors: an ancient chromophore serving trendy blue-light sensors.* Annu Rev Plant Biol, 2012. **63**: p. 49-72.

11. Otto, M.K., et al., *Replacement of riboflavin by an analogue in the blue-light photoreceptor of Phycomyces.* Proc Natl Acad Sci U S A, 1981. **78**(1): p. 266-9.

12. Mansurova, M., et al., *Chromophore exchange in the blue light-sensitive photoreceptor YtvA from Bacillus subtilis.* Chembiochem, 2011. **12**(4): p. 641-6.

13. Mataga, N., H. Chosrowjan, and Y. Shibata, *Ultrafast fluorescence quenching dynamics of flavin chromophores in protein nanospace.* J. Phys. Chem. B, 1998. **102**: p. 7081-7084.

14. van den Berg, P.A., et al., *Flavin fluorescence dynamics and photoinduced electron transfer in Escherichia coli glutathione reductase.* Biophys J., 1998. **74**(4): p. 2046-58.

15. Lakowicz, J.R., *Principles of fluorescence spectroscopy*. 3 ed. 2006: Springer.

References

16. Orlowska, M., et al., *Continuous and pulsed ultraviolet light for nonthermal treatment of liquid foods. Part 1: Effects on quality of fructose solution, apple juice, and milk.* Food and Bioprocess Technology, 2012. **6**(6): p. 1580-1592.

17. Díez-Pascual, A.M., et al., *Determination of riboflavin based on fluorescence quenching by graphene dispersions in polyethylene glycol.* RCS Adv., 2016. **6**: p. 19686.

18. Fraikin, G.Y., M.G. Strakhovskaya, and A.B. Rubin, *Biological photoreceptors of light-dependent regulatory processes.* Biochemistry (Mosc), 2013. **78**(11): p. 1238-53.

19. Liscum, E., D.W. Hodgson, and T.J. Campbell, *Blue light signaling through the cryptochromes and phototropins. So that's what the blues is all about.* Plant Physiol, 2003. **133**(4): p. 1429-36.

20. Herrou, J. and S. Crosson, *Function, structure and mechanism of bacterial photosensory LOV proteins.* Nat Rev Microbiol, 2011. **9**(10): p. 713-23.

21. Akbar, S., et al., *New family of regulators in the environmental signaling pathway which activates the general stress transcription factor sigma(B) of Bacillus subtilis.* J Bacteriol, 2001. **183**(4): p. 1329-38.

22. Moglich, A. and K. Moffat, *Structural basis for light-dependent signaling in the dimeric LOV domain of the photosensor YtvA.* J Mol Biol, 2007. **373**(1): p. 112-26.

23. Conrad, K.S., A.M. Bilwes, and B.R. Crane, *Light-induced subunit dissociation by a light-oxygen-voltage domain photoreceptor from Rhodobacter sphaeroides.* Biochemistry, 2013. **52**(2): p. 378-91.

24. Zoltowski, B.D. and B.R. Crane, *Light activation of the LOV protein vivid generates a rapidly exchanging dimer.* Biochemistry, 2008. **47**(27): p. 7012-9.

25. Song, S.H., et al., *Primary photochemistry of the dark- and light-adapted states of the YtvA protein from Bacillus subtilis.* Biochemistry, 2013. **52**(45): p. 7951-63.

26. Buttani, V., et al., *Conformational analysis of the blue-light sensing protein YtvA reveals a competitive interface for LOV-LOV dimerization and interdomain interactions.* Photochem Photobiol Sci, 2007. **6**(1): p. 41-9.

27. Dorn, M., et al., *LOV takes a pick: thermodynamic and structural aspects of the flavin-LOV-interaction of the blue-light sensitive photoreceptor YtvA from Bacillus subtilis.* PLoS One, 2013. **8**(11): p. e81268.

28. http://www.rcsb.org/pdb/home/home.do, 06/16/2016

29. Strickland, D., K. Moffat, and T.R. Sosnick, *Light-activated DNA binding in a designed allosteric protein.* Proc Natl Acad Sci U S A, 2008. **105**(31): p. 10709-14.

30.   Drepper, T., et al., *Reporter proteins for in vivo fluorescence without oxygen.* Nat Biotechnol, 2007. **25**(4): p. 443-5.

31.   Chapman, S., et al., *The photoreversible fluorescent protein iLOV outperforms GFP as a reporter of plant virus infection.* Proc Natl Acad Sci U S A, 2008. **105**(50): p. 20038-43.

32.   Christie, J.M., et al., *Structural tuning of the fluorescent protein iLOV for improved photostability.* J Biol Chem, 2012. **287**(26): p. 22295-304.

33.   Mukherjee, A., et al., *Engineering and characterization of new LOV-based fluorescent proteins from Chlamydomonas reinhardtii and Vaucheria frigida.* ACS Synth Biol, 2015. **4**(4): p. 371-7.

34.   Wingen, M., et al., *The photophysics of LOV-based fluorescent proteins - new tools for cell biology.* Photochem Photobiol Sci, 2014. **13**(6): p. 875-83.

35.   Buckley, A.M., et al., *LOV-based reporters for fluorescence imaging.* Curr Opin Chem Biol, 2015. **27**: p. 39-45.

36.   Losi, A., et al., *A photochromic bacterial photoreceptor with potential for super-resolution microscopy.* Photochem Photobiol Sci, 2013. **12**(2): p. 231-5.

37.   Greer, L.F., 3rd and A.A. Szalay, *Imaging of light emission from the expression of luciferases in living cells and organisms: a review.* Luminescence, 2002. **17**(1): p. 43-74.

38.   Wilson, T. and J.W. Hastings, *Bioluminescence.* Annu Rev Cell Dev Biol, 1998. **14**: p. 197-203.

39.   Cubitt, A.B., et al., *Understanding, improving and using green fluorescent proteins.* Trends Biochem Sci, 1995. **20**(11): p. 448-55.

40.   Hastings, J.W., *Bacterial bioluminescence.* Ann Rev Microbiol, 1977. **31**: p. 549-95.

41.   Lei, B., Q. Ding, and S.-C. Tu, *Identity of the emitter in the bacterial luciferase luminescence reaction: binding and fluorescence quantum yield studies of 5-decyl-4a-hydroxy-4a,5-dihydroriboflavin-5'-phosphate as a model.* Biochemistry, 2004. **43**: p. 15975-82.

42.   Tinikul, R. and P. Chaiyen, *Structure, mechanism, and mutation of bacterial luciferase.* Adv Biochem Eng Biotechnol, 2016. **154**: p. 47-74.

43.   Baldwin, T.O., et al., *Structure of bacterial luciferase.* Current Opinion in Structural Biology, 1995. **5**: p. 798-809.

44.   Miller, M.B. and B.L. Bassler, *Quorum sensing in bacteria.* Annu Rev Microbiol, 2001. **55**: p. 165-99.

45.   Hell, S.W. and J. Wichmann, *Breaking the diffraction resolution limit by stimulated emission - stimulated-emission-depletion fluorescence microscopy.* Opt Lett., 1994. **19**(11): p. 780-2.

References

46.   Betzig, E., et al., *Imaging intracellular fluorescent proteins at nanometer resolution.* Science, 2006. **313**(5793): p. 1642-5.

47.   Hess, S.T., T.P. Girirajan, and M.D. Mason, *Ultra-high resolution imaging by fluorescence photoactivation localization microscopy.* Biophys J, 2006. **91**(11): p. 4258-72.

48.   Rust, M.J., M. Bates, and X. Zhuang, *Sub-diffraction-limit imaging by stochastic optical reconstruction microscopy (STORM).* Nat Methods, 2006. **3**(10): p. 793-5.

49.   Dempsey, G.T., et al., *Evaluation of fluorophores for optimal performance in localization-based super-resolution imaging.* Nat Methods, 2011. **8**(12): p. 1027-36.

50.   Mortensen, K.I., et al., *Optimized localization analysis for single-molecule tracking and super-resolution microscopy.* Nat Methods, 2010. **7**(5): p. 377-81.

51.   Klar, T.A. and S.W. Hell, *Subdiffraction resolution in far-field fluorescence microscopy.* Opt Lett, 1999. **24**(14): p. 954-6.

52.   Hell, S.W., *Toward fluorescence nanoscopy.* Nat Biotechnol, 2003. **21**(11): p. 1347-55.

53.   Westphal, V. and S.W. Hell, *Nanoscale resolution in the focal plane of an optical microscope.* Phys Rev Lett, 2005. **94**(14): p. 143903.

54.   Wildanger, D., et al., *Solid immersion facilitates fluorescence microscopy with nanometer resolution and sub-angstrom emitter localization.* Adv Mater, 2012. **24**(44): p. OP309-13.

55.   Gottfert, F., et al., *Coaligned dual-channel STED nanoscopy and molecular diffusion analysis at 20 nm resolution.* Biophys J, 2013. **105**(1): p. L01-3.

56.   Hofmann, M., et al., *Breaking the diffraction barrier in fluorescence microscopy at low light intensities by using reversibly photoswitchable proteins.* Proc Natl Acad Sci U S A, 2005. **102**(49): p. 17565-9.

57.   Hell, S.W., L. Kastrup, and K.I. Willig, *STED microscopy sees details on the nanoscale.* Optics & Lasers Europe, 2007.

58.   https://www.ucl.ac.uk/super-resolution/images/STED_PSF, 07/01/2016

59.   Welsh, D.K. and T. Noguchi, *Cellular bioluminescence imaging.* Cold Spring Harb Protoc, 2012. **2012**(8).

60.   Close, D.M., et al., *In vivo bioluminescent imaging (BLI): noninvasive visualization and interrogation of biological processes in living animals.* Sensors (Basel), 2011. **11**(1): p. 180-206.

61.   Close, D.M., et al., *Comparison of human optimized bacterial luciferase, firefly luciferase, and green fluorescent protein for continuous imaging of cell culture and animal models.* J Biomed Opt, 2011. **16**(4): p. 047003.

62.   Isojima, Y., et al., *Ultraweak biochemiluminescence detected from rat hippocampal slices.* Neuroreport, 1995. **6**(4): p. 658-60.

63.   Agulhon, C., et al., *Bioluminescent imaging of Ca2+ activity reveals spatiotemporal dynamics in glial networks of dark-adapted mouse retina.* J Physiol, 2007. **583**(Pt 3): p. 945-58.

64.   Yamaguchi, S., et al., *Synchronization of cellular clocks in the suprachiasmatic nucleus.* Science, 2003. **302**: p. 1408-12.

65.   Mihalcescu, I., W. Hsing, and S. Leibler, *Resilient circadian oscillator revealed in individual cyanobacteria.* Nature, 2004. **430**(6995): p. 81-85.

66.   Karsi, A., S. Menanteau-Ledouble, and M.L. Lawrence, *Development of bioluminescent Edwardsiella ictaluri for noninvasive disease monitoring.* FEMS Microbiol Lett, 2006. **260**(2): p. 216-23.

67.   Nguyen, V.H., et al., *Genetically engineered Salmonella typhimurium as an imageable therapeutic probe for cancer.* Cancer Res, 2010. **70**(1): p. 18-23.

68.   http://www.olympus-lifescience.com/microscopes/inverted/lv200/, 06/08/2016

69.   Andresen, M., et al., *Photoswitchable fluorescent proteins enable monochromatic multilabel imaging and dual color fluorescence nanoscopy.* Nat Biotechnol, 2008. **26**(9): p. 1035-40.

70.   Stiel, A.C., et al., *Generation of monomeric reversibly switchable red fluorescent proteins for far-field fluorescence nanoscopy.* Biophys J, 2008. **95**(6): p. 2989-97.

71.   Grotjohann, T., et al., *Diffraction-unlimited all-optical imaging and writing with a photochromic GFP.* Nature, 2011. **478**(7368): p. 204-8.

72.   Brakemann, T., et al., *A reversibly photoswitchable GFP-like protein with fluorescence excitation decoupled from switching.* Nat Biotechnol, 2011. **29**(10): p. 942-7.

73.   Grotjohann, T., et al., *rsEGFP2 enables fast RESOLFT nanoscopy of living cells.* eLife, 2012: p. 1:e00248.

74.   Tiwari, D.K., et al., *A fast- and positively photoswitchable fluorescent protein for ultralow-laser-power RESOLFT nanoscopy.* Nat Methods, 2015. **12**(6): p. 515-8.

75.   Zhou, X.X. and M.Z. Lin, *Photoswitchable fluorescent proteins: ten years of colorful chemistry and exciting applications.* Curr Opin Chem Biol, 2013. **17**(4): p. 682-90.

References

76.   Danzl, J.G., et al., *Coordinate-targeted fluorescence nanoscopy with multiple off states.* Nat Photon, 2016. **10**: p. 122-8.

77.   McRae, S.R., C.L. Brown, and G.R. Bushell, *Rapid purification of EGFP, EYFP, and ECFP with high yield and purity.* Protein Expr Purif, 2005. **41**(1): p. 121-7.

78.   Patterson, G.H., et al., *Use of the green fluorescent protein and its mutants in quantitative fluorescence microscopy.* Biophys J, 1997. **73**: p. 2782-90.

79.   Silva, M.R., Jr., et al., *Photophysics of structurally modified flavin derivatives in the blue-light photoreceptor YtvA: a combined experimental and theoretical study.* Chembiochem, 2013. **14**(13): p. 1648-61.

80.   Yagur-Kroll, S. and S. Belkin, *Upgrading bioluminescent bacterial bioreporter performance by splitting the lux operon.* Anal Bioanal Chem, 2011. **400**(4): p. 1071-82.

81.   Close, D. M., et al., *Autonomous bioluminescent expression of the bacterial luciferase gene cassette (lux) in a mammalian cell line.* PLoS One, 2010. **5**(8), e12441

82.   Xu, T., et al., *Expression of a humanized viral 2A-mediated lux operon efficiently generates autonomous bioluminescence in human cells.* PLoS One, 2014. **9**(5): p. e96347.

83.   Sternberg, C., et al., *Detection of bioluminescence from individual bacterial cells a comparison of two different low-light imaging systems.* J Biolumin Chemilumin, 1997. **12**: p. 7-13.

84.   Westerlund-Karlsson, A., P. Saviranta, and M. Karp, *Generation of thermostable monomeric luciferases from Photorhabdus luminescens.* Biochem Biophys Res Commun, 2002. **296**(5): p. 1072-6.

85.   Shaner, N.C., P.A. Steinbach, and R.Y. Tsien, *A guide to choosing fluorescent proteins.* Nat Methods, 2005. **2**(12): p. 905-9.

86.   Ando, Y., et al., *Firefly bioluminescence quantum yield and colour change by pH-sensitive green emission.* Nat Photon, 2007. **2**(1): p. 44-47.

87.   Hall, M.P., et al., *Engineered luciferase reporter from a deep sea shrimp utilizing a novel imidazopyrazinone substrate.* ACS Chem Biol, 2012. **7**(11): p. 1848-57.

88.   Stacer, A.C., et al., *NanoLuc reporter for dual luciferase imaging in living animals.* Mol Imaging, 2013. **12**(7): p. 1-13.

89.   Nakajima, Y., et al., *Enhanced beetle luciferase for high-resolution bioluminescence imaging.* PLoS One, 2010. **5**(4): p. e10011.

90.   Patterson, S.S., et al., *Codon optimization of bacterial luciferase (lux) for expression in mammalian cells.* J Ind Microbiol Biotechnol, 2005. **32**(3): p. 115-23.

91. Bogosian, G. and E.V. Bourneuf, *A matter of bacterial life and death.* EMBO reports, 2001. **2**(9): p. 770-4.

92. Maglica, Z., E. Ozdemir, and J.D. McKinney, *Single-cell tracking reveals antibiotic-induced changes in mycobacterial energy metabolism.* MBio, 2015. **6**(1): p. e02236-14.

93. Olsson, O., et al., *Engineering of monomeric bacterial luciferases by fusion of luxA and luxB genes in Vibrio harveyi.* Gene, 1989. **81**(2): p. 335-47.

Acknowledgements

First of all, I would like to thank Prof. Stefan Hell for giving me the opportunity to work on these projects, for his encouragement and support of new ideas, and for providing an excellent lab environment.

I thank Prof. Anaclet Ngezahayo for his interest in this work and for being my doctoral supervisor and main referee.

In addition, I would like to thank Prof. Thomas Scheper for his willingness to be chair of the examination board.

I would also like to thank Dr. Klaus Gwosch, Dr. Sven Sidenstein, Dr. Johann Danzl, Dr. Martin Andresen, Dr. Katrin Willig, Dr. Waja Wegner, Dr. Heinz Steffens, Dr. Nicolai Urban, Dr. Douglas Richardson, Dr. Steffen Sahl, and Tanja Gilat for the great collaboration in these and other projects.

Furthermore, I would like to thank my office colleagues Joanna Oracz, Dr. Peter Ilgen, Dr. Franziska Stagge, Dr. Marlen Stäglich, Dr. Lena Große, Timo Konen, Isabelle Jansen, and Till Stephan for the nice time and helpful discussions.

In addition, I like to thank Dr. Björn Thiel and Dr. Heinz Steffens for the interesting conversations during lunch in the fresh air, even in snow and ice.

I also thank all my other colleagues for their helpfulness and the pleasant working atmosphere.

Special thanks go to Torsten Hartmann, Dr. Waja Wegner, Dr. Klaus Gwosch, Dr. Nicolai Urban, Dr. Sven Sidenstein, and Dr. Martin Andresen for the very fast proofreading of this manuscript.

Finally, I would like to thank my family, especially my parents and Torsten, for their support and encouragement.

Curriculum Vitae

Personal Details

Name:	Anne Carola Gregor
Date and place of birth:	December 18, 1986 in Hannover, Germany

School

1993-1997	Grundschule Ingeln-Oesselse
1997-1999	Orientierungsstufe Alte Rathausstraße Laatzen
Jan-Jul 1999	Orientierungsstufe Garbsen
1999-2006	Johannes-Kepler-Gymnasium Garbsen

Scientific Education

2006-2009	Bachelor of Science in Biochemistry Gottfried Wilhelm Leibniz Universität Hannover Bachelor thesis in the group of Prof. Dr. Dietmar Manstein, Institut für Biophysikalische Chemie, Medizinische Hochschule Hannover, Title: „Untersuchung der Wechselwirkung von EMD 57033 mit der Motordomäne von β-Myosin"
2009-2011	Master of Science in Biochemistry Medizinische Hochschule Hannover Master thesis in the group of Prof. Dr. Stefan Hell, Dept. of NanoBiophotonics, MPI for Biophysical Chemistry, Göttingen, Title: "Development of a Method for Two-Color Live Cell Imaging of Mammalian Cells with STED Microscopy"
Since 2011	Doctoral Studies in the group of Prof. Dr. Stefan Hell, Dept. of NanoBiophotonics, MPI for Biophysical Chemistry, Göttingen

List of Publications

Willig KI, Steffens H, Gregor C, Herholt A, Rossner MJ, Hell SW
Nanoscopy of filamentous actin in cortical dendrites of a living mouse
Biophysical Journal **106**(1), L01-L03 (2014)

Danzl JG*, Sidenstein SC*, Gregor C, Urban NT, Ilgen P, Jakobs S, Hell SW
Coordinate-targeted fluorescence nanoscopy with multiple off states
Nature Photonics **10**, 122-128 (2016)

Bader A, Bintig W, Begandt D, Klett A, Siller IG, Gregor C, Schaarschmidt F, Weksler B, Romero I, Couraud PO, Hell SW, Ngezahayo A
Adenosine receptors regulate gap junction coupling of the human cerebral microvascular endothelial cells hCMEC/D3 by Ca^{2+} influx through cyclic nucleotide-gated channels
The Journal of Physiology **595**(8), 2497-2517 (2017)

Winter FR, Loidolt M, Westphal V, Butkevich AN, Gregor C, Sahl SJ, Hell SW
Multicolour nanoscopy of fixed and living cells with a single STED beam and hyperspectral detection
Scientific Reports **7**, 46492 (2017)

Richardson DS*, Gregor C*, Winter FR, Urban NT, Sahl SJ, Willig KI, Hell SW
SRpHi ratiometric pH biosensors for super-resolution microscopy
Nature Communications **8**(1), 577 (2017)

Wegner W, Ilgen P, Gregor C, van Dort J, Mott AC, Steffens H, Willig KI
In vivo mouse and live cell STED microscopy of neuronal actin plasticity using far-red emitting fluorescent proteins
Scientific Reports **7**(1), 11781 (2017)

Gregor C, Gwosch KC, Sahl SJ, Hell SW
Strongly enhanced bacterial bioluminescence with the *ilux* operon for single-cell imaging
PNAS, **115**(5), 962-967 (2018)

Gregor C, Sidenstein SC, Andresen M, Sahl SJ, Danzl JG, Hell SW

Novel reversibly switchable fluorescent proteins for RESOLFT and STED nanoscopy engineered from the bacterial photoreceptor YtvA

Scientific Reports **8**(1), 2724 (2018)

* equal contributions